ASAR RNAs control replication through interactions with dozens of RNA binding proteins.

Mathew J. Thayer[1,*], Michael B. Heskett[2,4], Leslie G. Smith[1], Paul Spellman[2,3,], and Phillip A. Yates[1].

[1]Department of Chemical Physiology and Biochemistry
[2] Department of Molecular and Medical Genetics
[3]Cancer Early Detection Advanced Research Center, Knight Cancer Institute
Oregon Health & Science University
3181 S. W. Sam Jackson Park Road
Portland, Oregon 97239, USA

[4]Stanford Cancer Institute
291 Campus Drive, Stanford CA, 94305.

***Corresponding author.**

ORCID: 0000-0001-6483-1661

TEL: (503) 494-2447

FAX: (503) 494-7368

Email:thayerm@ohsu.edu

Abstract

ASARs are a family of very-long noncoding RNAs that control replication timing on individual human autosomes, and are essential for chromosome integrity. The eight known ASAR genes express RNAs that remain localized to their parent chromosomes. Analysis of eCLIP data revealed >30 nuclear matrix/RNA binding proteins (RBPs) that interact with multiple ASAR RNAs. An ~7kb domain within the ASAR6-141 RNA shows a striking density of RBP interaction sites. Genetic deletion and ectopic integration assays indicate that the ~7kb RNA binding protein domain contains functional sequences for controlling replication timing of entire chromosomes *in cis*. Depletion of 10 different ASAR-associated RBPs results in loss of the chromosome territory localization of ASAR RNAs, and alters the normal synchronous replication timing program on all human autosomes, recapitulating the effect of individual ASAR gene knockouts on a genome-wide scale. Our results indicate that ASAR RNAs serve as an essential RNA scaffold for the assembly of RBP complexes that function in normal chromosome replication and help maintain the structural integrity of each mammalian chromosome.

39 **Introduction:**

40 The vast majority of mammalian DNA replicates in homologous regions of
41 chromosome pairs in a highly synchronized manner (Dileep and Gilbert, 2018;
42 Mukhopadhyay et al., 2014; Rivera-Mulia et al., 2018). However, genetic disruption of
43 non-protein coding ASAR ("ASynchronous replication and Autosomal RNA") genes
44 causes a delay in replication timing on individual human chromosomes in *cis*, resulting in
45 highly asynchronous replication between pairs of autosomes (Donley et al., 2015; Heskett
46 et al., 2020; Heskett et al., 2022; Stoffregen et al., 2011). The first two ASAR genes were
47 identified at the breakpoints of human chromosome translocations that displayed a
48 chromosome-wide delay in replication timing that is associated with a chromosome-wide
49 delay in mitotic chromosome condensation [DRT/DMC; (Donley *et al.*, 2015; Stoffregen
50 *et al.*, 2011). ASAR RNAs are extremely long (>185 kb), and remain associated with the
51 chromosome territories where they are transcribed (Chang et al., 2007; Donley *et al.*,
52 2015; Donley et al., 2013; Platt et al., 2018; Stoffregen *et al.*, 2011). One unusual
53 characteristic of ASAR genes is that they are subject to an epigenetic program that results
54 in random Allelic Expression Imbalance [AEI; (Donley *et al.*, 2015; Heskett *et al.*, 2020;
55 Heskett et al., 2021; Heskett *et al.*, 2022; Stoffregen *et al.*, 2011)]. In addition, as the
56 name implies ASAR genes display epigenetically programmed ASynchronous
57 Replication Timing (ASRT) between alleles (Donley *et al.*, 2015; Heskett *et al.*, 2020;
58 Heskett *et al.*, 2022; Stoffregen *et al.*, 2011). Recently, we used these notable ASAR
59 characteristics to identify 69 additional ASAR gene candidates located on every human
60 autosome (Heskett *et al.*, 2020; Heskett *et al.*, 2022). The eight genetically validated
61 ASAR genes are located on human chromosomes 1, 6, 8, 9 and 15 (Donley *et al.*, 2015;

62 Heskett *et al.*, 2020; Heskett *et al.*, 2022; Stoffregen *et al.*, 2011). Altogether, these
63 findings suggest that ASARs represent ubiquitous essential *cis*-acting elements of
64 mammalian chromosome replication timing and structural integrity.

65 Chromosome-associated long non-protein coding RNAs are known to be important for
66 numerous aspects of chromosome dynamics in diverse eukaryotes from yeast to
67 mammals (Creamer et al., 2021; Ding et al., 2019; Faber and Vo, 2022; Menon and
68 Meller, 2015; Nozawa and Gilbert, 2019). The mammalian nucleus is rich in heterogenous
69 nuclear RNA (hnRNA), representing >95% of the total RNA Polymerase II output (Nozawa
70 and Gilbert, 2019; St Laurent et al., 2012). The vast majority of this hnRNA is poorly
71 defined, has been referred to as the "Dark Matter" of the genome (St Laurent *et al.*, 2012),
72 and includes spliced and unspliced intronic sequences, circular RNAs (Kristensen et al.,
73 2019), very long intergenic non-coding RNAs (vlincRNAs) (St Laurent et al., 2016), as
74 well as poorly defined RNAs that include chromatin associated RNAs [caRNAs; (Nozawa
75 et al., 2017)] and repeat rich RNAs that can be detected by C0t1 DNA [which is comprised
76 primarily of LINE and SINE sequences; reviewed in (Creamer *et al.*, 2021; Frank and
77 Rippe, 2020; Nozawa and Gilbert, 2019; St Laurent *et al.*, 2016)]. Some of these nuclear
78 RNAs have been studied extensively and comprise abundant species with defined
79 functions, while others are thought to be the by-products of other nuclear processes with
80 no known function and have been collectively called "RNA debris" (Nozawa and Gilbert,
81 2019).

82 Heterogeneous nuclear ribonucleoproteins (hnRNPs) represent a large family of
83 abundant RNA-binding proteins (RBPs) that contribute to multiple aspects of nucleic acid
84 metabolism. Many of the proteins that are in hnRNP complexes share general features,

85 but differ in domain composition and functional properties [reviewed in (Geuens et al.,
86 2016)]. The functions of hnRNPs vary according to their subcellular localization. Most of
87 the hnRNPs possess a conventional nuclear localization signal and are predominantly
88 present in the nucleus during steady state, where they function in various RNA metabolic
89 processes including transcription, splicing, and mRNA export [reviewed in (Geuens *et al.*,
90 2016)].

91 Here, we used publicly available eCLIP data from ENCODE (Moore et al., 2020) to
92 identify RBPs that interact with multiple ASAR RNAs, and found >30 different RBPs,
93 including HNRNPA1, HNRNPU, HNRNPUL1, HNRNPC, and HNRNPM, that interact with
94 three known ASARs. We also found that an ~7kb region within the ~185 kb ASAR6-141
95 RNA has a surprisingly high density of interacting RBPs, and that deletion of this ~7kb
96 "RBP domain" from the endogenous *ASAR6-141* gene results in a delayed replication
97 timing phenotype that is comparable to deletion of the entire ~185 kb *ASAR6-141* gene
98 on human chromosome 6. In addition, ectopic integration of transgenes expressing the
99 ~7kb RBP domain into autosomes or into the inactive X chromosome resulted in retention
100 of the RNA within the chromosome territory of the integrated chromosomes, and resulted
101 in delayed replication timing, delayed mitotic chromosome condensation, and
102 chromosome structure instability in *cis*. Taken together, these results indicate that the
103 ~7kb RBP domain represents a critical region within the *ASAR6-141* gene that controls
104 replication timing of human chromosome 6.

105 Previous studies found that siRNA mediated depletion, or forced expression of
106 dominant interfering mutants of HNRNPU resulted in dissociation of C0t1 and Xist RNAs
107 from their chromosome territories (Creamer *et al.*, 2021; Hall et al., 2014; Hasegawa et

108 al., 2010; Kolpa et al., 2021). Here we found that shRNA mediated depletion of 10
109 different ASAR-associated RBPs (HNRNPU, HNRNPC, HNRNPL, HNRNPUL1,
110 HNRNPM, HLTF, KHSRP, KHDRBS1, UCHL5, or TIA1/TIAL1) results in loss of the
111 chromosome territory localization of multiple ASAR RNAs. In addition, knockdown of
112 HNRNPU, HNRNPUL1, UCHL5, or TIA/TIAL1 dramatically altered the normal
113 synchronous replication timing program of all human autosome pairs, recapitulating the
114 effect of individual ASAR gene knockouts on a genome-wide scale.

115 Many recent studies have revealed a surprisingly dynamic and stochastic nature of
116 chromatin in eukaryotic nuclei, which is reminiscent of a multiphase fluid behavior
117 (Laghmach et al., 2021a; Laghmach et al., 2021b; Rippe, 2022). Disruption of this liquid-
118 liquid phase using brief exposure to 1,6-hexanediol results in alterations of higher order
119 chromatin organization in living cells (Liu et al., 2021; Ulianov et al., 2021). Here, we found
120 that a brief exposure to 1,6-hexanediol interfered with the chromosome territory
121 localization of multiple ASAR and C0T1 RNAs. In addition, we found that new RNA
122 synthesis is required for recovery of the chromosome territory association of C0t1 RNA
123 following 1,6-hexanediol exposure. In summary, these results indicate that ASAR RNAs
124 serve as an essential RNA scaffold for the assembly of RBP complexes that function in
125 normal chromosome replication timing, and in the maintenance of structural integrity of
126 each mammalian chromosome.

127

128 **Results**

129 We first sought to identify RBPs that interact with the known ASAR RNAs using
130 publicly available eCLIP data [see ENCODE; (Moore *et al.*, 2020)]. Using a strategy of

131 mapping the eCLIP RNA sequence reads to the human genome for >120 RBPs from two
132 different human cell lines, HEPG2 and K562, we identified dozens of RBPs that interact
133 with known ASAR RNAs (Table S1; also see Table S2). An example of the alignment of
134 the eCLIP RNAseq reads to the genomic region containing *ASAR6-141* is shown in Figure
135 1A, and also illustrates the genomic location of RNAseq reads from total RNA isolated
136 from both cell lines (also from ENCODE). Given the wide distribution of RNAseq reads
137 from total RNA that map to *ASAR6-141* in both cell lines, we were surprised to detect an
138 ~7 kb region that contained virtually all of the eCLIP sequences from both cell lines. In
139 total, we detected 693 independent eCLIP reads from 67 different RBPs in HEPG2 and
140 217 independent eCLIP reads from 55 RBPs in K562, with sequences from 33 different
141 RBPs being shared between the two cell lines, and all reads mapping to the ~7kb region
142 (see Tables S1 and S2). The zoomed in region in Figure 1A shows alignment of the eCLIP
143 sequences to the ~7kb RNA Binding Protein Domain (RBPD; see Table S1). In addition,
144 because K562 cells are female we could directly compare the RBPs that are shared
145 between the ~7kb RBPD and XIST RNA within the same eCLIP dataset. We found that
146 51 out of the 55 RBPs that are bound to the ~7kb RBPD in K562 cells are also bound to
147 XIST RNA (Tables S1 and S2).
148
149 **Disruption of the ~7kb RBPD within ASAR6-141 results in delayed replication.**
150 To determine if the ~7kb RBPD within the *ASAR6-141* gene contains replication timing
151 activity we used CRISPR/Cas9 mediated engineering to delete the ~7 kb sequence from
152 the endogenous locus. For this analysis we designed single guide RNAs (sgRNAs) to
153 unique sequences on either side of the ~7kb RBPD (see Fig. 1A). We expressed these

154 sgRNAs in combination with Cas9 in human HTD114 cells and screened clones for
155 deletion of the ~7kb RBPD (Fig. S1). We chose HTD114 cells for this analysis because
156 they maintain AEI and ASRT of both imprinted and random monoallelic genes, they have
157 a stable karyotype that does not change significantly following transfection, drug selection
158 and sub-cloning, and knockouts of the eight known ASAR genes, including ASAR6-141,
159 result in delayed replication timing, delayed mitotic condensation and chromosome
160 structure instability in *cis* (Breger et al., 2005; Chang *et al.*, 2007; Donley *et al.*, 2015;
161 Donley *et al.*, 2013; Heskett *et al.*, 2020; Heskett *et al.*, 2022; Platt *et al.*, 2018; Stoffregen
162 *et al.*, 2011). Because *ASAR6-141* expression is mono-allelic in the HTD114 cells
163 (Heskett *et al.*, 2020), we isolated clones that had heterozygous or homozygous deletions
164 of the ~7kb RBPD. We determined which alleles were deleted based on retention of the
165 different base pairs of heterozygous SNPs located within the ~7kb RBPD (see Fig. S1).
166 To assay replication timing of individual chromosomes we quantified DNA synthesis
167 in mitotic cells using a BrdU terminal label assay [Fig. 1B; and (Smith et al., 2001; Smith
168 and Thayer, 2012). In addition, the HTD114 cells contain a centromeric polymorphism on
169 chromosome 6, which allows for an unambiguous distinction between the two
170 chromosome 6 homologs [(Donley *et al.*, 2013; Platt *et al.*, 2018; Stoffregen *et al.*, 2011);
171 also see Fig. 1D and E]. From our previous studies we knew that the chromosome 6 with
172 the smaller centromere is linked to the expressed allele of *ASAR6-141* (Heskett *et al.*,
173 2020). For simplicity, we refer to the chromosome 6 with the larger centromere as 6A and
174 to the chromosome 6 with the smaller centromere as 6B. As expected, prior to disruption
175 of the ~7kb RBPD chromosomes 6A and 6B, as well as all other chromosome pairs
176 assayed, display synchronous replication [Fig. 1H; and see (Breger *et al.*, 2005; Donley

177 *et al.*, 2015; Donley *et al.*, 2013; Stoffregen *et al.*, 2011)]. Figure 1C-1D shows this
178 replication timing analysis on a mitotic cell where the ~7kb RBPD was deleted from the
179 expressed allele (CHR6B). Note that CHR6B contains more BrdU incorporation than
180 CHR6A (Fig. 1E-1G). Quantification of the BrdU incorporation in CHR6B and CHR6A in
181 multiple cells indicated that deletion of the expressed allele of the ~7kb RBPD resulted in
182 a significant delay in replication timing (Fig. 1H). This is in contrast to cells containing a
183 deletion of the ~7kb RBPD from the silent allele (CHR6A) where the BrdU incorporation
184 is comparable between CHR6B and CHR6A (Fig. 1H). A similar asynchronous replication
185 pattern between the chromosome 6 homologs was present in cells with homozygous
186 deletions, with CHR6B representing the later replicating allele (Fig. 1H). In addition, we
187 found that the delayed replication associated with deletion of the ~7kb RBPD on CHR6B
188 is comparable to the delayed replication associated with deletion of the entire *ASAR6-*
189 *141* gene from the same chromosome (Fig. 1H). These results indicate that the ~7kb
190 RBPD contains functional sequences for controlling replication timing, and that
191 expression of the ~7kb RBPD is important for controlling replication timing of chromosome
192 6.
193
194 **Ectopic integration of transgenes expressing the ~7kb RBPD into autosomes.**
195 To determine if the ~7 kb RBPD is sufficient to induce delayed replication in an
196 ectopic integration assay, we generated two transgenes containing the ~7kb RBPD, one
197 in the sense orientation and one in the antisense orientation with respect to the promoter
198 (Fig. 2A). These transgenes were introduced into mouse cells and individual clones
199 isolated. We initially screened individual clones for expression of the transgenes using

200 RNA FISH with the ~7kb RBPD as probe. Because the mouse cells that we used are
201 female, we included an RNA FISH probe for Xist to serve as positive control for the RNA
202 FISH assay. This two-color RNA FISH assay allowed us to identify clones with single sites
203 of transgene expression, and allowed us to directly compare the RNA FISH signals from
204 the transgenes to that of the endogenous Xist RNA hybridization signals expressed from
205 the inactive X chromosomes. Figure 2B shows examples of the RNA FISH signals in cells
206 expressing either the sense or antisense transgenes. Large clouds of RNA FISH
207 hybridization signals that are comparable to Xist RNA hybridization signals were detected
208 in 4 out of 12 clones expressing the sense transgene. In contrast, 0 out of 12 clones
209 expressing the antisense transgene expressed RNA FISH hybridization signals
210 comparable to Xist RNA signals, but instead only small pinpoint sites of RNA FISH
211 hybridization were detected (Fig. 2B). Note that some of the mouse cells are tetraploid
212 and therefore contain two Xist RNA hybridization signals.

213 To determine which mouse chromosomes contain the transgenes, we used DNA
214 FISH using the ~7kb RBPD DNA as probe in combination with the inverted DAPI banding
215 pattern to identify the mouse chromosomes in metaphase spreads. We then confirmed
216 the identity of the mouse chromosomes using DNA FISH on metaphase spreads using
217 the ~7kb RBPD in combination with a BAC probe from the chromosome of interest. For
218 example, clone ~7kb(+)A5, which contains the sense-strand transgene integrated in
219 mouse chromosome 5 is shown in Figure S2A. Next, to determine if the sense strand
220 RNA expressed from the ~7kb RBPD transgene is retained within the chromosome 5
221 territory, we used RNA-DNA FISH with the ~7kb RBPD as RNA probe plus a chromosome
222 paint to detect mouse chromosome 5 DNA in clone ~7kb(+)A5. Figure 2C shows that the

223 ~7kb RBPD RNA is localized to one of the chromosome 5s, indicating that the ~7kb RBPD
224 RNA is retained within the chromosome 5 territory.
225 Next to determine if the ~7kb RBPD transgene alters replication timing, we visualized
226 DNA synthesis in mitotic cells using a BrdU terminal label assay [see Fig. 1B; and (Smith
227 *et al.*, 2001; Smith and Thayer, 2012)]. In this assay, cells were exposed to BrdU for five
228 hours, harvested for mitotic cells, and processed for BrdU incorporation and for FISH
229 using the ~7kb RBPD transgene to identify the integrated chromosome. Figure 2D-E
230 shows an example of this replication-timing assay in a mitotic cell containing the ~7kb
231 RBPD sense transgene integrated into mouse chromosome 5. Note that the chromosome
232 containing the ~7kb RBPD transgene is delayed in mitotic condensation and contains
233 more BrdU incorporation than any other chromosome within the same cell. In contrast,
234 integration of transgenes with the ~7kb RBPD in the antisense orientation did not result
235 in delayed condensation nor in delayed replication of mouse chromosomes (see Fig. 2F
236 and 2G).
237
238 **Ectopic integration of the ~7kb RBPD transgene into the inactive X chromosome.**
239 Ectopic integration of *Xist* transgenes into autosomes has been an instrumental tool in
240 characterization of *Xist* functions, including the ability to delay replication timing and
241 induce gene silencing (Lee et al., 1996; Minks and Brown, 2009; Pintacuda et al., 2017).
242 We next sought to determine the consequences of ectopic integration of the ~7kb RBPD
243 into the inactive X chromosome. The ectopic integration assays described above involved
244 an RNA FISH screen for clones expressing the ~7kb RBPD, and included an RNA FISH
245 probe for Xist RNA as positive control. Therefore, to identify transgene integrations into

246 the inactive X chromosome, we simply screened an additional 50 clones for colocalization
247 of RNA FISH hybridization signals for both Xist and the ~7kb RBPD sense transgene.
248 Figure 3A shows this RNA FISH assay on cells where the Xist and ~7kb RBPD
249 hybridization signals are colocalized. We note that the intensity of the Xist RNA FISH
250 signal was enhanced in the area where the ~7kb RBPD hybridization signal was detected,
251 suggesting that the presence of the ~7kb RBPD RNA promoted preferential localization
252 of Xist RNA in the same region of the X chromosome territory that contains the ~7kb
253 RBPD RNA.

254 To confirm that the mouse X chromosome contains the transgene, we used DNA FISH
255 using the ~7kb RBPD DNA as probe in combination with an X chromosome paint probe
256 on metaphase spreads. An example of this analysis is shown in Figure S2B-2C, and
257 indicates that the ~7kb RBPD sense transgene is integrated into the X chromosome.
258 During this analysis we detected delayed mitotic condensation on X chromosomes, and
259 the X chromosomes with delayed mitotic condensation contain the ~7kb RBPD
260 transgene, an example of this analysis is shown in Figure 3C-3D.

261 Next to determine if the ~7kb RBPD transgene alters replication timing of the inactive
262 X chromosome, we visualized DNA synthesis in mitotic cells using our BrdU terminal label
263 assay (Smith *et al.*, 2001; Smith and Thayer, 2012). Figure 3E-3H shows an example of
264 this assay in a mitotic cell containing the ~7kb RBPD sense transgene integrated into the
265 inactive X chromosome. In this assay, cells were exposed to BrdU for five hours,
266 harvested for mitotic cells, and processed for BrdU incorporation and for FISH using the
267 ~7kb RBPD transgene plus an X chromosome paint probe to identify the integrated

268 chromosome. In summary, integration of the 7kb RBPD transgene was sufficient to cause
269 DRT/DMC on the inactive X chromosome.
270
271 **Depletion of RBPs disrupts the chromosome territory localization of ASAR RNAs.**
272 The results described above identified >2 dozen RBPs expressed in two different cell
273 lines that interact with an ~7kb domain within ASAR6-141 RNA, and that this ~7kb RBPD
274 is critical for controlling chromosome-wide DNA replication timing. We next used shRNA
275 knockdown of 13 RBPs that bind within the ~7kb RBPD plus 5 additional RBPs that
276 interact with two other ASAR RNAs and/or Xist RNA (see Table S1) to determine if these
277 RBPs function in the chromosome territory localization of ASAR RNAs. For this analysis
278 we used shRNA knockdown of the RBPs in HTD114 cells. Figure 4A shows the
279 quantification of HNRNPU by Western blot and by quantitative immunofluoresence
280 assays, and indicates an ~70% reduction in HNRNPU in both assays. Figure 4B shows
281 the RNA-DNA FISH for ASAR6-141 RNA in cells expressing empty vector and shows the
282 expected chromosome territory localized RNA FISH signal on one chromosome 6. In
283 contrast, depletion of HNRNPU resulted in a dramatic disruption of the ASAR6-141 RNA
284 hybridization signal into multiple punctate foci that are no longer associated with the
285 chromosome 6 DNA probe.
286 Next, to determine if the chromosomal localization of other ASARs was also affected
287 by HNRNPU knockdown we carried out RNA-DNA FISH for localization of ASAR1-187
288 and ASAR6 RNAs simultaneously. For this analysis we used Fosmid probes to detect the
289 ASAR RNAs plus BAC probes to detect the DNA for the ASAR genes located on
290 chromosomes 1 and 6. Figure 4D shows the RNA-DNA FISH assay on cells expressing

291 empty vector, and indicates that the RNA FISH signals for both ASARs are closely
292 associated with their DNA FISH signals on the two different chromosomes. In contrast,
293 cells with HNRNPU knockdown showed a dispersed punctate nuclear pattern for both
294 ASAR RNAs, and that the punctate foci show overlapping hybridization signals for both
295 ASAR RNAs. In addition to the punctate nuclear pattern of RNA localization following
296 HNRNPU depletion, we also detected cells with cytoplasmic localization of ASAR1-187
297 and ASAR6 RNAs (Fig. 4F-4G). This cytoplasmic localization was also detected for
298 ASAR6-141 RNA (not shown). Similar results were obtained following shRNA depletion
299 of HNRNPC, HNRNPL, HNRNPUL1, HNRNPM, HLTF, KHSRP, KHDRBS1, UCHL5,
300 TIA1/TIAL1 (Fig. S3). In contrast, shRNA depletion of SAFB, SAFB2, SAFB plus SAFB2,
301 HNRNPA1, or CTCF did not affect ASAR RNA localization (Fig. S4).
302
303 **Depletion of RBPs causes asynchronous replication on all autosomes.**
304 Next to determine if ASAR associated RBPs function during the normally synchronous
305 replication timing program between pairs of homologous chromosomes, we analyzed
306 DNA synthesis in mitotic cells depleted for HNRNPU, HNRNPUL1, UCHL5 or TIA1/TIAL1
307 using the BrdU terminal label assay [Fig. 1B; and (Smith *et al.*, 2001; Smith and Thayer,
308 2012)]. Figure 5 shows this analysis in cells that have been depleted for HNRNPU.
309 Analysis of cells prior to RBP depletion indicated that each autosome pair displays a
310 stereotypical and synchronous BrdU incorporation pattern for each autosome pair (Fig.
311 5A). In contrast, following HNRNPU depletion individual mitotic spreads displayed
312 dramatic differential incorporation of BrdU into pairs of homologous chromosomes. Figure
313 5B shows examples of asynchronous replication timing between every pairs of autosome.

314 Note that each chromosome pair contains dramatic differential BrdU incorporation
315 between homologs that represents considerable asynchronous replication timing. Figure
316 5C-5E shows three examples of the chromosome pairs 1, 4 and 18. Quantification of the
317 BrdU incorporation in chromosomes 1 and 6 in multiple cells depleted for HNRNPU or
318 TIA1/TIAL1 indicated that each pair of chromosomes displays significant asynchrony (Fig.
319 5F). In addition, ~1/3 of all mitotic spreads contained one or a few chromosomes that
320 displayed the full delay in replication timing/delay in mitotic chromosome condensation
321 (DRT/DMC) phenotype (two examples are shown in Fig. 5G-5H).
322
323 **A brief exposure to 1,6 hexanediol disrupts ASAR and C0t1 RNA localization.**
324 Recent studies have found that a brief exposure to 1,6-hexanediol results in alterations
325 of higher order chromatin organization in living cells, which is consistent with disruption
326 of a liquid-liquid phase separation [LLPS; see (Liu *et al.*, 2021; Ulianov *et al.*, 2021)]. The
327 shRNA depletion assays described above resulted in mislocalization of multiple ASAR
328 RNAs into punctate foci, which is suggestive of liquid-liquid phase separation. To
329 determine if 1,6-hexanediol can disrupt the chromosome territory localization of ASAR
330 RNAs we exposed HTD114 cells to 4% 1,6-hexanediol for 20 minutes, and then
331 processed the cells for RNA-DNA FISH. Figure 6 shows this analysis and indicates that
332 the chromosome territory localization of ASAR6 and ASAR6-141 RNA is disrupted in cells
333 exposed to 1,6-hexanediol, with both RNAs being detected as a diffuse hybridization
334 pattern in the nucleus and cytoplasm. In addition, washing out the 1,6-hexanediol and
335 allowing the cells to recover for 4 hours revealed that the ASAR RNAs regained their
336 normal chromosome territory localization pattern (Fig. 6D and 6G).

337 Next to determine if exposure to 1,6-hexanediol can also disrupt the chromosome
338 territory localization of C0t1 RNA we exposed HA(4)A cells, which are mouse A9 hybrid
339 cells containing human chromosome 4, to 4% 1,6-hexanediol for 20 minutes and then
340 processed the cells for RNA-DNA FISH. Figure 7 shows this analysis and indicates that
341 the chromosome territory localization of hCot1 RNA is disrupted in cells exposed to 1,6-
342 hexanediol, and that the hC0t1 RNA is detected as a diffuse hybridization pattern in the
343 nucleus and cytoplasm (Fig. 7B). In addition, washing out the 1,6-hexanediol and allowing
344 the cells to recover for 4 hours revealed that the hC0t1 RNA regained its normal
345 chromosome territory association pattern (Fig. 7C). To determine if new RNA synthesis
346 is required to reestablish the chromosome territory localization of hC0t1 RNA, we treated
347 cells with 1,6-hexanediol for 20 minutes, washed out the 1,6-hexanediol and allowed the
348 cells to recover for 4 hours either in the presence or absence of Actinomycin D. Figure
349 7D-7E shows this analysis and indicates that hC0t RNA was not detected on the human
350 chromosome territory in the presence of Actinomycin D, indicating that new RNA
351 synthesis is required for the generation of chromosome territory localization of C0t1 RNA.
352

353 **Discussion:**

354 We recently identified 69 ASAR candidate genes, and genetically validated 6 out of 6 as
355 controlling replication timing of individual chromosomes, bringing the total of genetically
356 validated ASAR genes to eight (Heskett *et al.*, 2020; Heskett *et al.*, 2022). The eight ASAR
357 genes (*ASAR1-187, ASAR6, ASAR6-141, ASAR8-2.7, ASAR9-23, ASAR9-24, ASAR9-*
358 *30 and ASAR15*) display striking epigenetically controlled AEI, ASRT and their RNAs
359 remain localized to their parent chromosome territories (Donley *et al.*, 2015; Heskett *et*

360 *al.*, 2020; Heskett *et al.*, 2022; Stoffregen *et al.*, 2011). Evidence that ASAR RNA
361 mediates the chromosome-wide effects on replication timing came from oligonucleotide
362 mediated RNA degradation of ASAR6 RNA that was expressed from a BAC transgene
363 integrated into a mouse chromosome, thus reversing the chromosome-wide delayed
364 replication timing induced by the *ASAR6* transgene (Platt *et al.*, 2018). In this report, we
365 used publicly available RNA-protein interaction data from ENCODE in combination with
366 a strategy of mapping the eCLIP sequences to the human genome to identify >30 nuclear
367 matrix/RBPs that interact with multiple ASAR RNAs. One unanticipated observation that
368 came from this analysis was that an ~7kb domain within the ~185kb ASAR6-141 RNA
369 contained virtually all of the RBP interaction sites for >30 different RBPs in two different
370 human cell lines. Using genetic deletion and ectopic integration assays we found that the
371 ~7kb RBPD contains functional sequences for controlling replication timing of entire
372 chromosomes in *cis*. We also found that shRNA-mediated depletion of 10 different ASAR-
373 associated RBPs results in loss of the chromosome territory association of multiple ASAR
374 RNAs. In addition, we found that depletion of HNRNPU, HNRNPUL1, UCHL5, and
375 TIA/TIAL1 alters the normally synchronous replication timing that occurs between pairs
376 of homologous chromosomes, recapitulating the effect of individual ASAR gene
377 knockouts on a genome-wide scale. Furthermore, we found that a brief exposure of cells
378 to 1,6-hexanediol disrupts the chromosome territory localization of multiple ASAR RNAs
379 as well as C0t1 RNA, and that new RNA synthesis is required to restore the chromosome
380 territory localization of C0t1 RNA.

381 Previous studies have suggested that long nascent transcripts that are detected by
382 C0t1 DNA play a dynamic structural role that promotes the open architecture of active

383 chromosome territories (Creamer *et al.*, 2021; Hall *et al.*, 2014). The RNA species
384 detected by C0t1 DNA are predominantly L1 sequences, and these L1 RNAs remain
385 associated with the chromosome territories where they are made (Hall *et al.*, 2014).
386 Additional studies have described repetitive RNA (repRNA) as important regulators of the
387 dynamic organization of genomic loci into membrane-less subcompartments with distinct
388 nuclear functions [reviewed in (Frank and Rippe, 2020)]. Recent studies have also
389 proposed that abundant nuclear proteins such as HNRNPU nonspecifically interact with
390 "RNA debris" that creates a dynamic nuclear mesh that regulates interphase chromatin
391 structure (Nozawa *et al.*, 2017; Nozawa and Gilbert, 2019). One important distinction that
392 can be made between ASARs and these other hnRNAs [i.e. C0t1 RNA, repRNA, caRNA,
393 and "RNA debris" (Creamer *et al.*, 2021; Frank and Rippe, 2020; Hall *et al.*, 2014; Kolpa
394 *et al.*, 2021; Nozawa *et al.*, 2017; Nozawa and Gilbert, 2019)] is that ASARs are defined
395 genetically, and these other RNAs are not. Thus, we have used both loss of function and
396 gain of function assays to define the roles that ASARs play in chromosome dynamics,
397 which includes control of chromosome-wide replication timing and mitotic chromosome
398 condensation (Donley *et al.*, 2015; Donley *et al.*, 2013; Heskett *et al.*, 2020; Heskett *et*
399 *al.*, 2022; Platt *et al.*, 2018; Stoffregen *et al.*, 2011). We also note that C0t1 DNA, when
400 used as an RNA FISH probe, can detect ASAR6 RNA that is expressed and localized to
401 an individual chromosome territory (Figure S4), indicating that at least some of the RNA
402 FISH signal detected by C0T1 DNA represents ASARs. In addition, we found that a brief
403 exposure to 1,6-hexanediol disrupts the chromosome territory localization of multiple
404 ASAR RNAs, suggesting that ASAR RNAs participate in the nuclear LLPS processes that
405 organize chromosome territories. Given our recent discovery of ASAR candidate genes

406 on every autosome, representing ~3% of the human genome (Heskett *et al.*, 2022), we
407 propose that the functional "chromosome associated RNA" species that control
408 chromosome dynamics within mammalian nuclei are encoded by ASAR genes. Whether
409 or not there are nuclear functions of "RNA debris" that are independent of ASARs will
410 require genetic and/or functional validation.

411 Here we identified several hnRNPs (HNRNPU, HNRNPUL1, HNRNPC, and HNRNPM)
412 as important interaction partners for the chromosome territory localization of ASAR RNAs.
413 In addition, we found that the KH domain (HNRNPK Homology domain) containing
414 proteins KHSRP and KHDRBS1 also contribute to the chromosome territory localization
415 of ASAR RNAs. We also found that depletion of HNRNPU, HNRNPUL1, UCHL5, and
416 TIA1/TIAL1 proteins resulted in a dramatic genome-wide disruption of the normally
417 synchronous replication timing program on all autosome pairs. Taken together our results
418 indicate that the association of ASAR RNAs with hnRNPs and nuclear matrix associated
419 proteins is an essential step in the regulation of the replication timing program on
420 mammalian chromosomes.

421

422

423 **References:**

424 Breger, K.S., Smith, L., and Thayer, M.J. (2005). Engineering translocations with
425 delayed replication: evidence for cis control of chromosome replication timing. Hum Mol
426 Genet *14*, 2813-2827.
427 Chang, B.H., Smith, L., Huang, J., and Thayer, M. (2007). Chromosomes with delayed
428 replication timing lead to checkpoint activation, delayed recruitment of Aurora B and
429 chromosome instability. Oncogene *26*, 1852-1861.
430 Creamer, K.M., Kolpa, H.J., and Lawrence, J.B. (2021). Nascent RNA scaffolds
431 contribute to chromosome territory architecture and counter chromatin compaction. Mol
432 Cell. 10.1016/j.molcel.2021.07.004.
433 Dileep, V., and Gilbert, D.M. (2018). Single-cell replication profiling to measure
434 stochastic variation in mammalian replication timing. Nature communications *9*, 427.
435 10.1038/s41467-017-02800-w.
436 Ding, D.Q., Okamasa, K., Katou, Y., Oya, E., Nakayama, J.I., Chikashige, Y., Shirahige,
437 K., Haraguchi, T., and Hiraoka, Y. (2019). Chromosome-associated RNA-protein
438 complexes promote pairing of homologous chromosomes during meiosis in
439 Schizosaccharomyces pombe. Nature communications *10*, 5598. 10.1038/s41467-019-
440 13609-0.
441 Donley, N., Smith, L., and Thayer, M.J. (2015). ASAR15, A cis-Acting Locus that
442 Controls Chromosome-Wide Replication Timing and Stability of Human Chromosome
443 15. PLoS Genet *11*, e1004923. 10.1371/journal.pgen.1004923.
444 Donley, N., Stoffregen, E.P., Smith, L., Montagna, C., and Thayer, M.J. (2013).
445 Asynchronous Replication, Mono-Allelic Expression, and Long Range Cis-Effects of
446 ASAR6. PLoS Genet *9*, e1003423.
447 Faber, M.W., and Vo, T.V. (2022). Long RNA-Mediated Chromatin Regulation in Fission
448 Yeast and Mammals. Int J Mol Sci *23*. 10.3390/ijms23020968.
449 Frank, L., and Rippe, K. (2020). Repetitive RNAs as Regulators of Chromatin-
450 Associated Subcompartment Formation by Phase Separation. J Mol Biol *432*, 4270-
451 4286. 10.1016/j.jmb.2020.04.015.
452 Geuens, T., Bouhy, D., and Timmerman, V. (2016). The hnRNP family: insights into
453 their role in health and disease. Hum Genet *135*, 851-867. 10.1007/s00439-016-1683-5.
454 Hall, L.L., Carone, D.M., Gomez, A.V., Kolpa, H.J., Byron, M., Mehta, N., Fackelmayer,
455 F.O., and Lawrence, J.B. (2014). Stable C0T-1 repeat RNA is abundant and is
456 associated with euchromatic interphase chromosomes. Cell *156*, 907-919.
457 10.1016/j.cell.2014.01.042.
458 Hasegawa, Y., Brockdorff, N., Kawano, S., Tsutui, K., Tsutui, K., and Nakagawa, S.
459 (2010). The matrix protein hnRNP U is required for chromosomal localization of Xist
460 RNA. Dev Cell *19*, 469-476. 10.1016/j.devcel.2010.08.006.
461 Heskett, M.B., Smith, L.G., Spellman, P., and Thayer, M.J. (2020). Reciprocal
462 monoallelic expression of ASAR lncRNA genes controls replication timing of human
463 chromosome 6. RNA (New York, N.Y.) *26*, 724-738. 10.1261/rna.073114.119.
464 Heskett, M.B., Spellman, P.T., and Thayer, M.J. (2021). Differential Allelic Expression
465 among Long Non-Coding RNAs. Non-coding RNA *7*. 10.3390/ncrna7040066.
466 Heskett, M.B., Vouzas, A.E., Smith, L.G., Yates, P.A., Boniface, C., Bouhassira, E.E.,
467 Spellman, P.T., Gilbert, D.M., and Thayer, M.J. (2022). Epigenetic Control of Hundreds

468 of Chromosome-Associated lncRNA Genes Essential for Replication and Stability.
469 bioRxiv, 2022.2004.2025.489405. 10.1101/2022.04.25.489405.
470 Kolpa, H.J., Creamer, K.M., Hall, L.L., and Lawrence, J.B. (2021). SAF-A mutants
471 disrupt chromatin structure through dominant negative effects on RNAs associated with
472 chromatin. Mamm Genome. 10.1007/s00335-021-09935-8.
473 Kristensen, L.S., Andersen, M.S., Stagsted, L.V.W., Ebbesen, K.K., Hansen, T.B., and
474 Kjems, J. (2019). The biogenesis, biology and characterization of circular RNAs. Nat
475 Rev Genet *20*, 675-691. 10.1038/s41576-019-0158-7.
476 Kruskal, J.B. (1964). Multidimensional scaling by optimizing goodness of fit to a
477 nonmetric hypothesis. Psychometrika *29*, 1–27.
478 Laghmach, R., Di Pierro, M., and Potoyan, D. (2021a). A Liquid State Perspective on
479 Dynamics of Chromatin Compartments. Front Mol Biosci *8*, 781981.
480 10.3389/fmolb.2021.781981.
481 Laghmach, R., Di Pierro, M., and Potoyan, D.A. (2021b). The interplay of chromatin
482 phase separation and lamina interactions in nuclear organization. Biophys J *120*, 5005-
483 5017. 10.1016/j.bpj.2021.10.012.
484 Lee, J.T., Strauss, W.M., Dausman, J.A., and Jaenisch, R. (1996). A 450 kb transgene
485 displays properties of the mammalian X-inactivation center. Cell *86*, 83-94.
486 Liu, X., Jiang, S., Ma, L., Qu, J., Zhao, L., Zhu, X., and Ding, J. (2021). Time-dependent
487 effect of 1,6-hexanediol on biomolecular condensates and 3D chromatin organization.
488 Genome Biol *22*, 230. 10.1186/s13059-021-02455-3.
489 Menon, D.U., and Meller, V.H. (2015). Identification of the Drosophila X chromosome:
490 The long and short of it. RNA biology *12*, 1088-1093. 10.1080/15476286.2015.1086864.
491 Minks, J., and Brown, C.J. (2009). Getting to the center of X-chromosome inactivation:
492 the role of transgenes. Biochem Cell Biol *87*, 759-766.
493 Moore, J.E., Purcaro, M.J., Pratt, H.E., Epstein, C.B., Shoresh, N., Adrian, J., Kawli, T.,
494 Davis, C.A., Dobin, A., Kaul, R., et al. (2020). Expanded encyclopaedias of DNA
495 elements in the human and mouse genomes. Nature *583*, 699-710. 10.1038/s41586-
496 020-2493-4.
497 Mukhopadhyay, R., Lajugie, J., Fourel, N., Selzer, A., Schizas, M., Bartholdy, B., Mar,
498 J., Lin, C.M., Martin, M.M., Ryan, M., et al. (2014). Allele-specific genome-wide profiling
499 in human primary erythroblasts reveal replication program organization. PLoS Genet *10*,
500 e1004319. 10.1371/journal.pgen.1004319.
501 Nozawa, R.S., Boteva, L., Soares, D.C., Naughton, C., Dun, A.R., Buckle, A.,
502 Ramsahoye, B., Bruton, P.C., Saleeb, R.S., Arnedo, M., et al. (2017). SAF-A Regulates
503 Interphase Chromosome Structure through Oligomerization with Chromatin-Associated
504 RNAs. Cell *169*, 1214-1227.e1218. 10.1016/j.cell.2017.05.029.
505 Nozawa, R.S., and Gilbert, N. (2019). RNA: Nuclear Glue for Folding the Genome.
506 Trends Cell Biol *29*, 201-211. 10.1016/j.tcb.2018.12.003.
507 Pintacuda, G., Wei, G., Roustan, C., Kirmizitas, B.A., Solcan, N., Cerase, A., Castello,
508 A., Mohammed, S., Moindrot, B., Nesterova, T.B., and Brockdorff, N. (2017). hnRNPK
509 Recruits PCGF3/5-PRC1 to the Xist RNA B-Repeat to Establish Polycomb-Mediated
510 Chromosomal Silencing. Mol Cell *68*, 955-969.e910. 10.1016/j.molcel.2017.11.013.
511 Platt, E.J., Smith, L., and Thayer, M.J. (2018). L1 retrotransposon antisense RNA within
512 ASAR lncRNAs controls chromosome-wide replication timing. J Cell Biol *217*, 541-553.
513 10.1083/jcb.201707082.

514 Rippe, K. (2022). Liquid-Liquid Phase Separation in Chromatin. Cold Spring Harb
515 Perspect Biol *14*. 10.1101/cshperspect.a040683.
516 Rivera-Mulia, J.C., Dimond, A., Vera, D., Trevilla-Garcia, C., Sasaki, T., Zimmerman, J.,
517 Dupont, C., Gribnau, J., Fraser, P., and Gilbert, D.M. (2018). Allele-specific control of
518 replication timing and genome organization during development. Genome Res *28*, 800-
519 811. 10.1101/gr.232561.117.
520 Smith, L., Plug, A., and Thayer, M. (2001). Delayed Replication Timing Leads to
521 Delayed Mitotic Chromosome Condensation and Chromosomal Instability of
522 Chromosome Translocations. Proc Natl Acad Sci U S A *98*, 13300-13305.
523 Smith, L., and Thayer, M. (2012). Chromosome replicating timing combined with
524 fluorescent in situ hybridization. J Vis Exp *10*, e4400.
525 St Laurent, G., Savva, Y.A., and Kapranov, P. (2012). Dark matter RNA: an intelligent
526 scaffold for the dynamic regulation of the nuclear information landscape. Frontiers in
527 genetics *3*, 57. 10.3389/fgene.2012.00057.
528 St Laurent, G., Vyatkin, Y., Antonets, D., Ri, M., Qi, Y., Saik, O., Shtokalo, D., de Hoon,
529 M.J., Kawaji, H., Itoh, M., et al. (2016). Functional annotation of the vlinc class of non-
530 coding RNAs using systems biology approach. Nucleic Acids Research. 2 *44*, 3233-
531 3252. 10.1093/nar/gkw162.
532 Stoffregen, E.P., Donley, N., Stauffer, D., Smith, L., and Thayer, M.J. (2011). An
533 autosomal locus that controls chromosome-wide replication timing and mono-allelic
534 expression. Hum Mol Genet *20*, 2366-2378.
535 Ulianov, S.V., Velichko, A.K., Magnitov, M.D., Luzhin, A.V., Golov, A.K., Ovsyannikova,
536 N., Kireev, II, Gavrikov, A.S., Mishin, A.S., Garaev, A.K., et al. (2021). Suppression of
537 liquid-liquid phase separation by 1,6-hexanediol partially compromises the 3D genome
538 organization in living cells. Nucleic Acids Research. 2 *49*, 10524-10541.
539 10.1093/nar/gkab249.
540 Zhu, Y., Bye, S., Stambrook, P.J., and Tischfield, J.A. (1994). Single-base deletion
541 induced by benzo[a]pyrene diol epoxide at the adenine phosphoribosyltransferase locus
542 in human fibrosarcoma cell lines. Mutat Res *321*, 73-79.
543
544

Figure legends

Figure 1. RNA binding proteins interact with an~7kb domain within ASAR6-141 RNA. A) Integrative Genomics Viewer view showing the genomic location of *ASAR6-141*. The genomic locations of RNAseq and eCLIP reads from HEPG2 and K562 (from ENCODE) are shown. The zoomed in view shows the ~7kb RBPD with the location of all of the eCLIP reads that map within the region (see Table S2). The location of sgRNAs are shown, the asterisks mark the sgRNAs from (Heskett *et al.*, 2020). B) Schematic illustration of the BrdU terminal label protocol(Smith and Thayer, 2012). Cells were treated with BrdU (green) for 5.5 hours and then harvested for mitotic cells. C-H) BrdU incorporation in HTD114 cells containing a heterozygous deletion of the the ~7kb RBPD. Cells containing a deletion of the ~7kb RBPD from the expressed allele of *ASAR6-141* were exposed to BrdU, harvested for mitotic cells, and subjected to DNA FISH using chromosome 6 centromeric probe (red; D-E). The larger centromere resides on the chromosome 6 with the silent *ASAR6-141* allele (6A), and the smaller centromere resides on the chromosome 6 with the expressed *ASAR6-141* allele (6B). DNA was stained with DAPI (blue). Bar is 10 uM. F and G) DAPI staining and BrdU incorporation were quantified by calculating the number of pixels (area x intensity) and displayed as a ratio of BrdU incorporation in chromosome 6B divided by the BrdU incorporation in chromosome 6A. H) Quantification of BrdU incorporation in multiple cells with heterozygous (∆7kb-6B, expressed allele; or ∆7kb-6A, silent allele) or homozygous (∆7kb-6B/6A) deletions of the ~7kb RBPD. Also included is the quantification of BrdU incorporation in heterozygous deletions of the entire ~185kb ASAR6-141 gene from chromosome 6B (∆185-6B) or 6A (∆185-6A) (Heskett *et al.*, 2020). **P = 0.00027 and *P = 0.03.

Figure 2. Replication timing in mouse cells containing *ASAR6-141 ~7kb RBPD* transgenes. A) Schematic view of the ~7kb RBPD in both the sense and antisense orientation. The promoter used to drive expression is from the ASAR6 gene (Platt *et al.*, 2018). B) Two color RNA FISH assay for expression of the ~7kb RBPD transgenes. Individual clones were screened for expression of the ASAR6-141 (~7kb RBPD) transgenes (red). RNA hybridization using an Xist probe (green) was used as positive control. The left and right panels represent examples of clones containing the sense and antisense transgenes, respectively. The arrows mark the ASAR6-141 RNA. C) RNA from the ~7kb RBPD remains localized to mouse chromosomes. RNA-DNA FISH using the ~7kb RBPD as RNA FISH probe (red), plus a mouse chromosome 5 paint to detect chromosome 5 DNA (green). D and E) Cells containing the sense ~7kb RBPD transgene integrated into mouse chromosome 5 were exposed to BrdU (green), harvested for mitotic cells, and subjected to DNA FISH using the ~7kb RBPD (red). Note that the chromosome that contains the transgene shows delayed mitotic condensation and more BrdU incorporation than any other chromosome within the same cell. F-G) Cells containing the antisense ~7kb RBPD transgene integrated into mouse chromosomes were exposed to BrdU (green), harvested for mitotic cells, and subjected to DNA FISH using the ~7kb RBPD (red). Note that the chromosome that contains the transgene shows normal mitotic condensation and only a small amount of BrdU incorporation.

591 **Figure 3. Replication timing in mouse cells containing *ASAR6-141 ~7kb RBPD***
592 **transgene integrated into the inactive X chromosome.** A) Two color RNA FISH assay
593 for expression of the sense ~7kb RBPD transgene plus Xist RNA. Individual clones were
594 screened for expression of the sense strand ~7kb RBPD transgene (red) in combination
595 with RNA FISH for Xist (green). Examples of three different cells showing colocalization
596 of the ASAR RNA and Xist RNA. The white lines show the path for the pixel intensity
597 profiles in panel B. B) Pixel intensity profiles across the Xist RNA hybridization domain
598 showing enhanced signal intensity over the ~7kb RBPD RNA hybridization domain. C and
599 D) Delayed mitotic chromosome condensation of the X chromosome that contains the
600 ~7kb RBPD transgene. An example of a mitotic spread processed for DNA FISH using
601 the ~7kb RBPD as probe (magenta) plus a mouse X chromosome paint (red). The arrows
602 mark the location of the transgene hybridization signal. E-H) Cells containing the sense
603 ~7kb RBPD transgene integrated into the mouse X chromosome were exposed to BrdU
604 (green), harvested for mitotic cells, and subjected to DNA FISH using the ~7kb RBPD
605 (magenta) plus a mouse X chromosome paint. Note that the chromosome that contains
606 the transgene (arrows) displays delayed mitotic condensation and more BrdU
607 incorporation than any other chromosome within the same cell.
608
609 **Figure 4. Depletion of HNRNPU results in disruption of the chromosome territory**
610 **localization of ASAR RNAs.** A) Quantitation of HNRNPU by Western blot (top) and by
611 quantitative immunofluorescence (bottom). B and C) RNA-DNA FISH for ASAR6-141
612 RNA. HTD114 cells were transfected with empty vector (B) or vector expressing an
613 shRNA against HNRNPU (C). The white arrows mark the RNA FISH signals and the
614 arrowheads mark the DNA FISH signals. B) Examples of three different nuclei showing
615 the RNA hybridization pattern for ASAR6-141 RNA in cells transfected with empty vector.
616 C) The top and bottom panels show examples of two different nuclei showing a punctate
617 RNA hybridization pattern for ASAR6-141 RNA in cells that were depleted for HNRNPU.
618 D-H) RNA-DNA FISH for ASAR1-187 and ASAR6 in cells depleted for HNRNPU. D)
619 Examples of nuclei from cells transfected with empty vector. The white arrows mark the
620 RNA FISH signals for ASAR6 (red) and ASAR1-187 (green). The DNA FISH signals for
621 *ASAR6* DNA (orange) and *ASAR1-187* (magenta) are marked with colored arrows as
622 shown. The merged image shows that the RNA and DNA FISH signals are adjacent to
623 each other. E) RNA FISH image showing a punctate nuclear pattern for ASAR6 RNA
624 (red) and ASAR1-187 RNA (green). The merged image shows that the FISH signal for
625 both ASARs are colocalized. F-H) RNA-DNA FISH showing cytoplasmic localization of
626 ASAR6 and ASAR1-187 RNAs. The white arrows mark the sites of colocalization of
627 ASAR6 and ASAR1-187 RNA in punctate foci in the cytoplasm. The FISH signals for
628 *ASAR6* DNA (orange) and *ASAR1-187* DNA (magenta) are marked with colored arrows
629 as shown. DNA was stained with DAPI, and Bars are 10*u*m.
630
631 **Figure 5. Depletion of HNRNPU results in asynchronous replication on autosome**
632 **pairs.** A) BrdU incorporation in parental HTD114 cells. Cells were exposed to BrdU for
633 five hours, processed for BrdU incorporation using an antibody against BrdU. This panel
634 represents chromosomes from multiple mitotic spreads showing representative BrdU
635 incorporation in chromosome. Each autosome pair were captured from the same mitotic
636 cell, and each pair displays a stereotypical BrdU incorporation pattern that is consistent

with synchronous replication timing. B) HTD114 cells were transfected with the HNRNPU shRNA expression vector, exposed to BrdU for five hours, and processed for BrdU incorporation. This panel represents chromosomes from multiple mitotic spreads showing representative BrdU incorporation in pairs of autosomes. Each autosome pair were captured from the same mitotic cell, and each pair displays a differential BrdU incorporation pattern that is consistent with asynchronous replication timing. C) Shows two chromosome 1 homologs side by side. For each CHR1 homolog (A or B) we show the inverted DAPI staining (black and white), chromosome 1 centromeric probe (red), BrdU incorporation (green), and DAPI staining (blue). Panels D and E show the BrdU incorporation in chromosomes 4 (CHR4A and CHR4B) and 18 (CHR18A and CHR18B), respectively. For each chromosome pair the inverted DAPI staining (black and white), BrdU incorporation (green), and DAPI staining (blue) are shown. Quantification of BrdU incorporation in multiple cells indicated that HNRNPU or TIA/TIAL1 depletion resulted in significant asynchrony ($P < 1 \times 10^{-5}$) between chromosome 1 and chromosome 6 homologs. The P values are form the Kruskal-Wallis test (Kruskal, 1964). G) DRT/DMC on chromosome 6 following HNRNPU depletion. HTD114 cells were transfected with the HNRNPU shRNA expression vector, exposed to BrdU for 5 hours, harvested for mitotic cells, and processed for BrdU incorporation (green) and DNA FISH using a chromosome 6 centromeric probe (red). H) DRT/DMC on chromosome 1 following UCHL5 depletion. HTD114 cells were transfected with the UCHL5 shRNA expression vector, exposed to BrdU for 5 hours, harvested for mitotic cells, and processed for BrdU incorporation (green) and DNA FISH using a chromosome 1 paint as probe (red). The arrow marks the chromosome 1 with DRT/DMC, and the inset shows only the DAPI staining of the chromosome 1 highlighting the DMC.

Figure 6. 1,6 hexanediol disrupts the chromosome territory association of ASAR RNAs. HTD114 cells were exposed to 4% 1,6 hexanediol (HD) for 20 minutes, washed extensively and allowed to recover for 4 hours in complete media, and processed for RNA-DNA FISH. A-C) RNA FISH using an ASAR6-141 probe plus a BAC probe from the ASAR6 locus to detect DNA. D-F) RNA FISH using an ASAR6 probe plus a BAC probe from the ASAR6 locus to detect DNA. Panels A and D are HTD114 cells prior to exposure. B and E) HTD114 cells exposed to HD for 20 minutes. C and F) HTD114 cells exposed to HD for 20 minutes followed by 4 hour incubation in the absence of HD (4hr washout).

Figure 7. 1,6 hexanediol disrupts the chromosome territory association of C0t1 RNA. HA(4)A cells were exposed to 4% 1,6 hexanediol (HD) for 20 minutes, washed extensively and allowed to recover for 4 hours in complete media, and processed for RNA-DNA FISH using C0t1 as probe from both RNA and DNA. A) Control HA(4)A cells prior to HD exposure. B) HA(4)A cells exposed to HD for 20 minutes. C) HA(4)A cells exposed to HD for 20 minutes, washed extensively and allowed to recover for 4 hours in complete media. D and E) HA(4)A cells exposed to HD for 20 minutes, washed extensively and allowed to recover for 4 hours in complete media containing Actinomycin D (ActD). F) Control HA(4)A cells exposed to Actinomycin D for 4 hours.

Figure S1. CRISPR/Cas9 deletion of the ~7kb RBPD. A) Integrative Genomics Viewer view showing the genomic location of *ASAR6-141*. The genomic locations of RNAseq

683 and eCLIP reads from HEPG2 and K562 (from ENCODE) are shown. The zoomed in
684 view shows the ~7kb RBPD with the location of all of the eCLIP reads that map within the
685 region (see Table S2). The location of sgRNAs that flank the ~7kb RBPD are shown. The
686 location of PCR primers (1-6) and the heterozygous SNP rs17070386 are also shown. B)
687 Sanger sequencing traces on PCR products generated from genomic DNA using primers
688 5 and 6 (see Table S3). In previous studies we generated mouse monochromosomal
689 hybrid cells containing the two chromosome 6 homologs, and sequencing traces from
690 these two hybrids, containing either chromosome 6A (CHR6A) or chromosome 6B
691 (CHR6B) are shown below the HTD114 panel. Sequencing traces from PCR products
692 generated from 4 heterozygous deletions, two with CHR6A deletions {D6A(7-82-29) and
693 D6A(7-82-13)} and two with CHR6B deletions {D6B(7-18-1) and D6B(7-63-1)} are shown.
694 C) Junction PCR (primers 1 and 4) on genomic DNA isolated from heterozygous {D6A(7-
695 82-29), D6A(7-82-13), D6B(7-18-1) and D6B(7-63-1)} or homozygous deletions {D6B/6A-
696 1 and D6B/6A-2} are shown. Parental HTD114 DNA was used as control. D) Internal PCR
697 products (primers 5 and 6) on genomic DNA isolated from heterozygous {D6A(7-82-29),
698 D6A(7-82-13), D6B(7-18-1) and D6B(7-63-1)} or homozygous deletions {D6B/6A-1 and
699 D6B/6A-2} are shown. Parental HTD114 DNA was used as control.
700
701 **Figure S2. Identification of mouse chromosomes containing the ~7kb RBPD**
702 **transgene.** A) DNA FISH on mouse chromosomes from clone ~7kb(+)A5. Mitotic spread
703 showing DNA FISH using the ~7kb RBPD (magenta; marked with arrows) and a mouse
704 chromosome 5 BAC (RP24-107D17; red; marked with arrowheads). B and C) DNA FISH
705 on mouse chromosomes from clone ~7kb(+)X1. Mitotic spread showing DNA FISH using
706 the ~7kb RBPD (magenta; marked with arrows) and a mouse X chromosome paint (red).
707
708 **Figure S3. Disruption of the chromosome territory localization of ASAR1-187 and**
709 **ASAR6 RNAs following shRNA depletion of RBPs.** HTD114 cells were transfected
710 with empty vector (A) or shRNA expression vectors for KHSRP (B), HNRNPL (C),
711 HNRNPUL1 (D), UCHL5 (E), KHDRBS1 (F), HTLF (G), HNRNPC (H), or TIA/TIAL1 (note
712 that the single knockdowns of TIA or TIAL1 did not disrupt ASAR RNA localization, not
713 shown). Cells were processed for RNA FISH using Fosmid probes (see Table S3) for
714 ASAR1-187 (green) and ASAR6 (red).
715
716 **Figure S4. RNA FISH on cells depleted for RBPs that did not disrupt ASAR**
717 **localization.** HTD114 cells were transfected with shRNA expression vectors for SAFB
718 (A), SAFB2 (B), SAFB and SAFB2 (C), HNRNPA1 (D), CTCF (E), or empty vector (F).
719 Cells were processed for RNA FISH using Fosmid probes (see Table S3) for ASAR1-187
720 (green) and ASAR6 (red).
721
722 **Figure S5. Human C0t1 DNA detects ASAR6 RNA.** Mouse cells containing an *ASAR6*
723 BAC (RP11-767E7) transgene integrated into mouse chromosome 3 were previously
724 described (Donley *et al.*, 2013). A-C) RNA-DNA FISH using and ASAR6 fosmid probe to
725 ASAR6 RNA (green; arrows) plus a mouse chromosome 3 paint probe to detect DNA
726 (red; arrowheads). D-F) RNA-DNA FISH using human C0t1 DNA to detect RNA (green;
727 arrows) plus the *ASAR6* BAC (red arrowheads) to detect DNA.
728

730 **STAR Methods**

731 *Cell culture*

732 HTD114 cells are a human *APRT* deficient cell line derived from HT1080 cells (Zhu et
733 al., 1994). Mouse C2C12 cells were used for the transgene integration assays, transfected
734 using Lipofectamine 2000 (Invitrogen) according to the manufacturer's recommendations,
735 and clones containing transgene integrations were isolated following selection in media
736 containing G418. All cells were grown in DMEM (Gibco) supplemented with 10% fetal
737 bovine serum (Hyclone), and were grown in a humidified incubator at 37°C in a 5% carbon
738 dioxide atmosphere.

739

740 *shRNA depletion of RBPs*

741 Using Lipofectamine 2000 (Invitrogen), according to the manufacturer's
742 recommendations, we co-transfected HTD114 cells with plasmids encoding puromycin
743 resistance (PGK-PURO) and shRNAs against 18 different RBPs (Millipore/Sigma). 24h
744 after transfection, cells were plated in media containing 10 ug/ml puromycin
745 (Millipore/Sigma), and 24h-48h following puromycin selection cells were processed for
746 Western blot, RNA-DNA FISH or for replication timing assays (see below).

747

748 *Western blot analysis*

749

750 *CRISPR/Cas9 engineering*

751 Using Lipofectamine 2000 (Invitrogen), according to the manufacturer's
752 recommendations, we co-transfected HTD114 cells with plasmids encoding GFP,

753 sgRNAs and Cas9 endonuclease (Origene). Each plasmid encoded sgRNA was designed
754 to bind at the indicated locations (Figure S1). 48h after transfection, cells were plated at
755 clonal density and allowed to expand for 2-3 weeks. The presence of deletions was
756 identified by PCR using the primers described in Figure S1. The single cell colonies that
757 grew were analyzed for heterozygous deletions by PCR (Figure S1). We used retention
758 of a heterozygous SNP to identify the disrupted allele, and homozygosity at the SNP
759 confirmed that cell clones were homogenous.
760
761 *PCR analysis*
762 Genomic DNA was isolated from tissue culture cells using TRIZOL Reagent
763 (Invitrogen). PCR was performed in a 12.5μL volume using 50-100ng of genomic DNA,
764 1x Standard Taq Buffer (New England Biolabs, Inc.), 200μM each deoxynucleotide
765 triphosphates, 0.2μM of each primer, and 3 units of Taq DNA Polymerase (New England
766 Biolabs, Inc.) under the following reaction conditions: 95°C for 2 minutes, followed by 30-
767 40 cycles of 95°C for 30 seconds, 55-62°C for 45 seconds, and 72°C for 1 minute, with a
768 final extension time of 10 minutes at 72°C. PCR products were separated on 1% agarose
769 gels, stained with ethidium bromide, and photographed under ultraviolet light illumination.
770 Sequencing of PCR products was carried out at the Vollum Institute DNA Sequencing
771 Core facility.
772
773 *DNA FISH*
774 Mitotic chromosome spreads were prepared as described previously (Smith *et al.*,
775 2001). After RNase (100μg/ml) treatment for 1h at 37°C, slides were washed in 2XSSC

776 and dehydrated in an ethanol series and allowed to air dry. Chromosomal DNA on the
777 slides was denatured at 75°C for 3 minutes in 70% formamide/2XSSC, followed by
778 dehydration in an ice-cold ethanol series and allowed to air dry. BAC and Fosmid DNAs
779 were labeled using nick translation (Vysis, Abbott Laboratories) with Spectrum Orange-
780 dUTP, Spectrum Aqua-dUTP or Spectrum Green-dUTP (Vysis). Final probe
781 concentrations varied from 40-60 ng/µl. Centromeric probe cocktails (Vysis) and/or whole
782 chromosome paint probes (Metasystems) plus BAC or Fosmid DNAs were denatured at
783 75°C for 10 minutes and prehybridized at 37°C for 10 minutes. Probes were applied to
784 denatured slides and incubated overnight at 37°C. Post-hybridization washes consisted of
785 one 3-minute wash in 50% formamide/2XSSC at 40°C followed by one 2-minute rinse in
786 PN (0.1M Na_2HPO_4, pH 8.0/2.5% Nonidet NP-40) buffer at RT. Coverslips were mounted
787 with Prolong Gold antifade plus DAPI (Invitrogen) and viewed under UV fluorescence
788 (Olympus).
789
790 *RNA-DNA FISH*
791 Cells were plated on Poly-L-Lysine coated (Millipore Singa) glass microscope slides
792 at ~50% confluence and incubated for 4 hours in complete media in a 37°C humidified
793 CO_2 incubator. Slides were rinsed 1X with sterile RNase free PBS. Cell Extraction was
794 carried out using ice cold solutions as follows: Slides were incubated for 30 seconds in
795 CSK buffer (100mM NaCl/300mM sucrose/3mM $MgCl_2$/10mM PIPES, pH 6.8), 10 minutes
796 in CSK buffer/0.1% Triton X-100, followed by 30 seconds in CSK buffer. Cells were then
797 fixed in 4% paraformaldehyde in PBS for 10 minutes and stored in 70% EtOH at -20°C
798 until use. Just prior to RNA FISH, slides were dehydrated through an EtOH series and

799 allowed to air dry. Denatured probes were prehybridized at 37°C for 10 min, applied to
800 non-denatured slides and hybridized at 37ºC for 14-16 hours. Post-hybridization washes
801 consisted of one 3-minute wash in 50% formamide/2XSSC at 40˚C followed by one 2-
802 minute rinse in 2XSSC/0.1% TX-100 for 1 minute at RT. Slides were then fixed in 4%
803 paraformaldehyde in PBS for 5 minutes at RT, and briefly rinsed in 2XSSC/0.1% TX-100
804 at RT. Coverslips were mounted with Prolong Gold antifade plus DAPI (Invitrogen) and
805 slides were viewed under UV fluorescence (Olympus). Z-stack images were generated
806 using a Cytovision workstation. After capturing RNA FISH signals, the coverslips were
807 removed, the slides were dehydrated in an ethanol series, and then processed for DNA
808 FISH, beginning with the RNase treatment step, as described above.
809
810 *Chromosome replication timing assay*
811 The BrdU replication timing assay was performed as described previously on
812 exponentially dividing cultures and asynchronously growing cells (Smith and Thayer,
813 2012). Mitotic chromosome spreads were prepared and DNA FISH was performed as
814 described above. The incorporated BrdU was then detected using a FITC-labeled anti-
815 BrdU antibody (Roche). Coverslips were mounted with Prolong Gold antifade plus DAPI
816 (Invitrogen), and viewed under UV fluorescence. All images were captured with an
817 Olympus BX Fluorescent Microscope using a 100X objective, automatic filter-wheel and
818 Cytovision workstation. Individual chromosomes were identified with either chromosome-
819 specific paints, centromeric probes, BACs or by inverted DAPI staining. Utilizing the
820 Cytovision workstation, each chromosome was isolated from the metaphase spread and
821 a line drawn along the middle of the entire length of the chromosome. The Cytovision

822 software was used to calculate the pixel area and intensity along each chromosome for
823 each fluorochrome occupied by the DAPI and BrdU (FITC) signals. The total amount of
824 fluorescent signal in each chromosome was calculated by multiplying the average pixel
825 intensity by the area occupied by those pixels. The BrdU incorporation into human
826 chromosomes containing CRISPR/Cas9 modifications was calculated by dividing the total
827 incorporation into the chromosome with the deleted chromosome divided by the BrdU
828 incorporation into the non-deleted chromosome within the same cell. Boxplots were
829 generated from data collected from 8-12 cells per clone or treatment group. Differences
830 in measurements were tested across categorical groupings by using the Kruskal-Wallis
831 test (Kruskal, 1964) and listed as P-values for the corresponding plots.
832
833

RESOURCE AVAILABILITY

Further information and requests for resources and reagents should be directed to and will be fulfilled by the lead contact, Mathew Thayer (thayerm@ohsu.edu)

Materials availability statement

All reagents generated in this study will be made freely available upon request.

Acknowledgments:

M.J.T. was supported by NIH NIGMS (R01GM114162 and R01GM130703).

M.B.H was supported by NIH NCI 4K00CA245677-03

Author contributions:

Declaration of interests

The authors declare no competing interests.

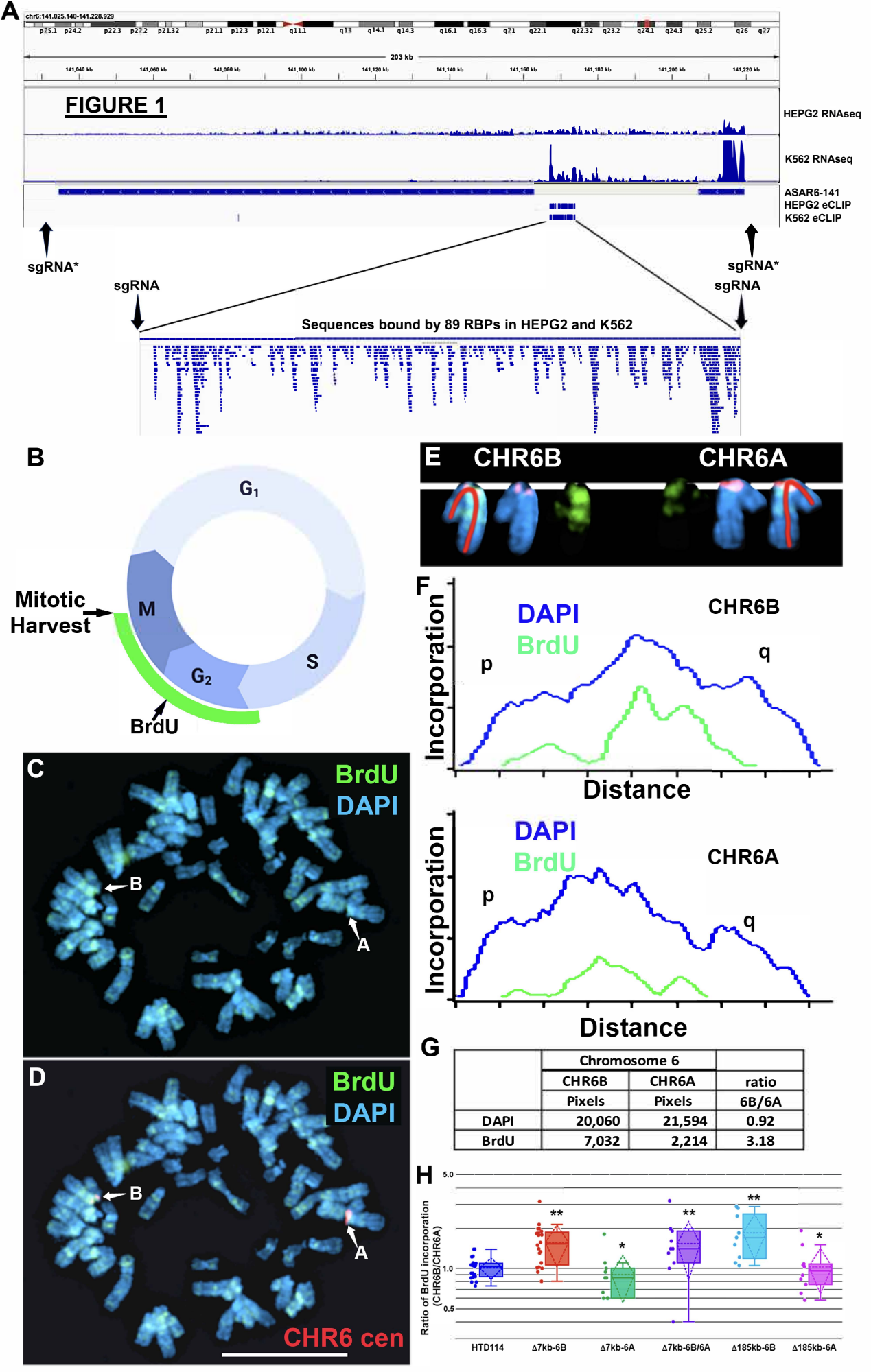

	Chromosome 6		
	CHR6B	CHR6A	ratio
	Pixels	Pixels	6B/6A
DAPI	20,060	21,594	0.92
BrdU	7,032	2,214	3.18

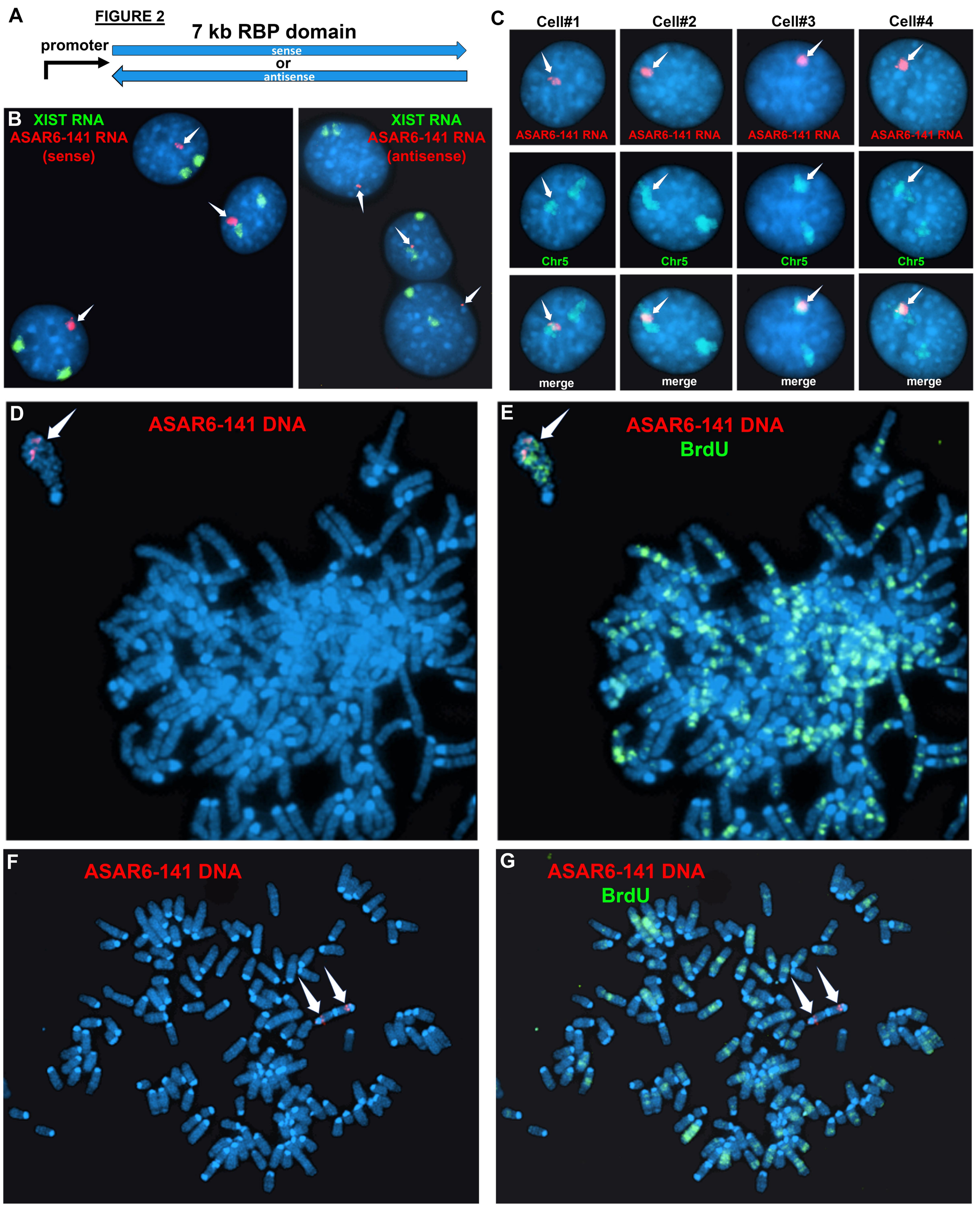
A
FIGURE 2
7 kb RBP domain
promoter
sense
or
antisense
B
XIST RNA
ASAR6-141 RNA
(sense)
XIST RNA
ASAR6-141 RNA
(antisense)
C
Cell#1
Cell#2
Cell#3
Cell#4
ASAR6-141 RNA
Chr5
merge
D
ASAR6-141 DNA
E
ASAR6-141 DNA
BrdU
F
ASAR6-141 DNA
G
ASAR6-141 DNA
BrdU

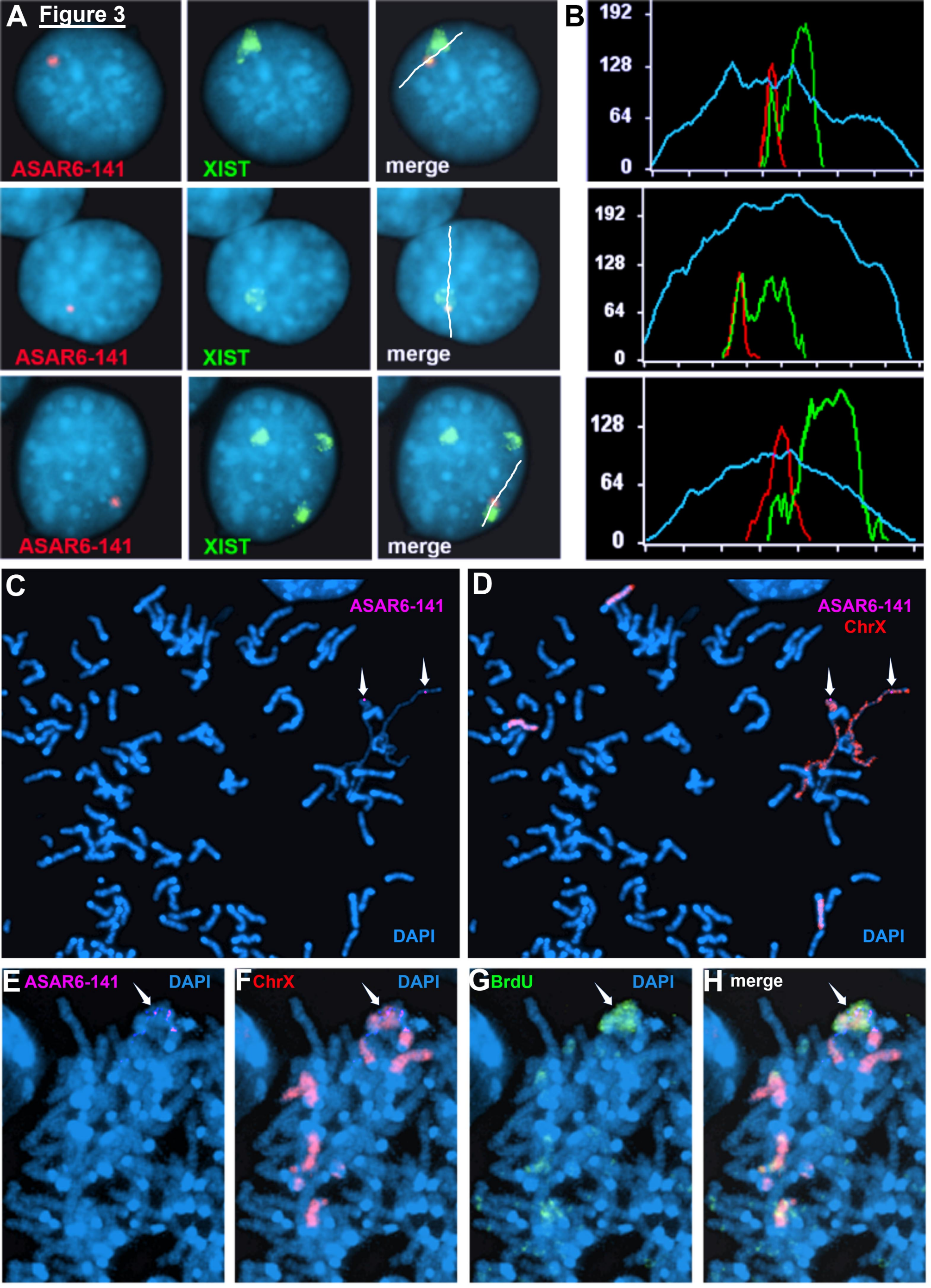
A
Figure 3
ASAR6-141
XIST
merge
B
192
128
64
0
C
ASAR6-141
DAPI
D
ASAR6-141
ChrX
DAPI
E
ASAR6-141
DAPI
F
ChrX
DAPI
G
BrdU
DAPI
H
merge

FIGURE 4

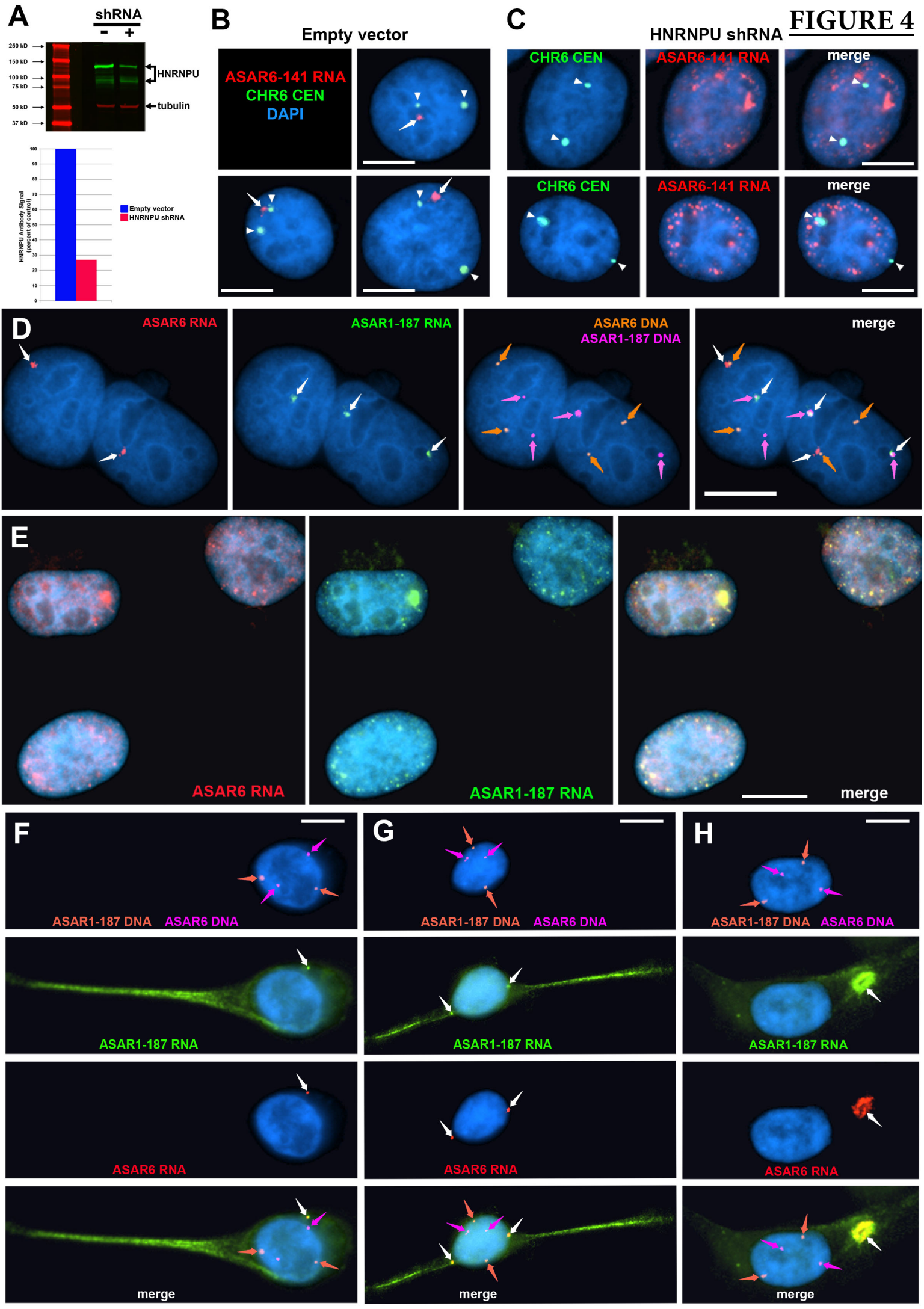
A
shRNA
-
+
250 kD
150 kD
100 kD
75 kD
50 kD
37 kD
HNRNPU
tubulin
HNRNPU Antibody Signal (percent of control)
Empty vector
HNRNPU shRNA
B
Empty vector
ASAR6-141 RNA
CHR6 CEN
DAPI
C
HNRNPU shRNA
CHR6 CEN
ASAR6-141 RNA
merge
D
ASAR6 RNA
ASAR1-187 RNA
ASAR6 DNA
ASAR1-187 DNA
merge
E
ASAR6 RNA
ASAR1-187 RNA
merge
F
G
H
ASAR1-187 DNA
ASAR6 DNA
ASAR1-187 RNA
ASAR6 RNA
merge

FIGURE 5

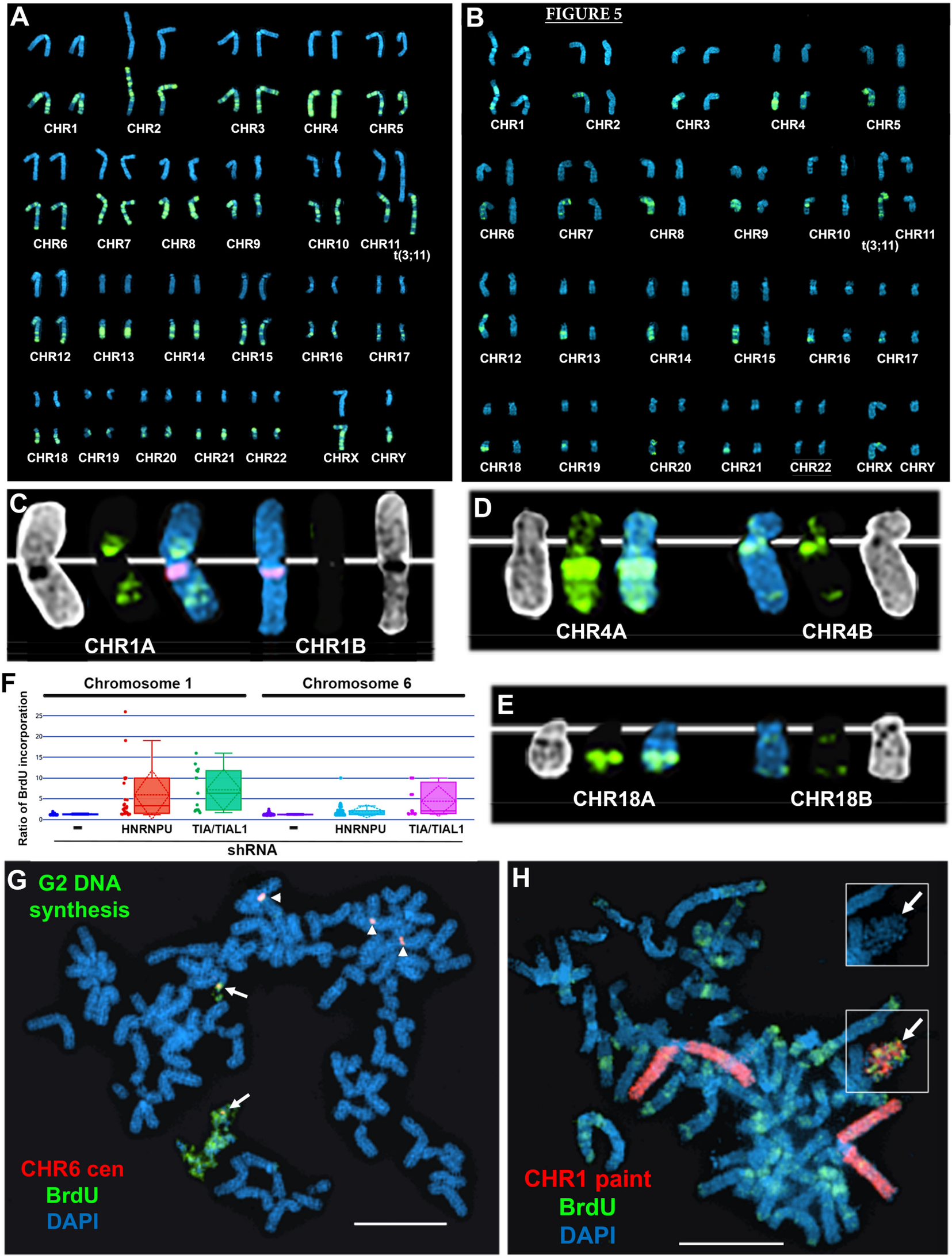
A
CHR1
CHR2
CHR3
CHR4
CHR5
CHR6
CHR7
CHR8
CHR9
CHR10
CHR11
t(3;11)
CHR12
CHR13
CHR14
CHR15
CHR16
CHR17
CHR18
CHR19
CHR20
CHR21
CHR22
CHRX
CHRY
B
CHR1
CHR2
CHR3
CHR4
CHR5
CHR6
CHR7
CHR8
CHR9
CHR10
CHR11
t(3;11)
CHR12
CHR13
CHR14
CHR15
CHR16
CHR17
CHR18
CHR19
CHR20
CHR21
CHR22
CHRX
CHRY
C
CHR1A
CHR1B
D
CHR4A
CHR4B
E
CHR18A
CHR18B
F
Chromosome 1
Chromosome 6
Ratio of BrdU incorporation
25
20
15
10
5
0
-
HNRNPU
TIA/TIAL1
-
HNRNPU
TIA/TIAL1
shRNA
G
G2 DNA synthesis
CHR6 cen
BrdU
DAPI
H
CHR1 paint
BrdU
DAPI

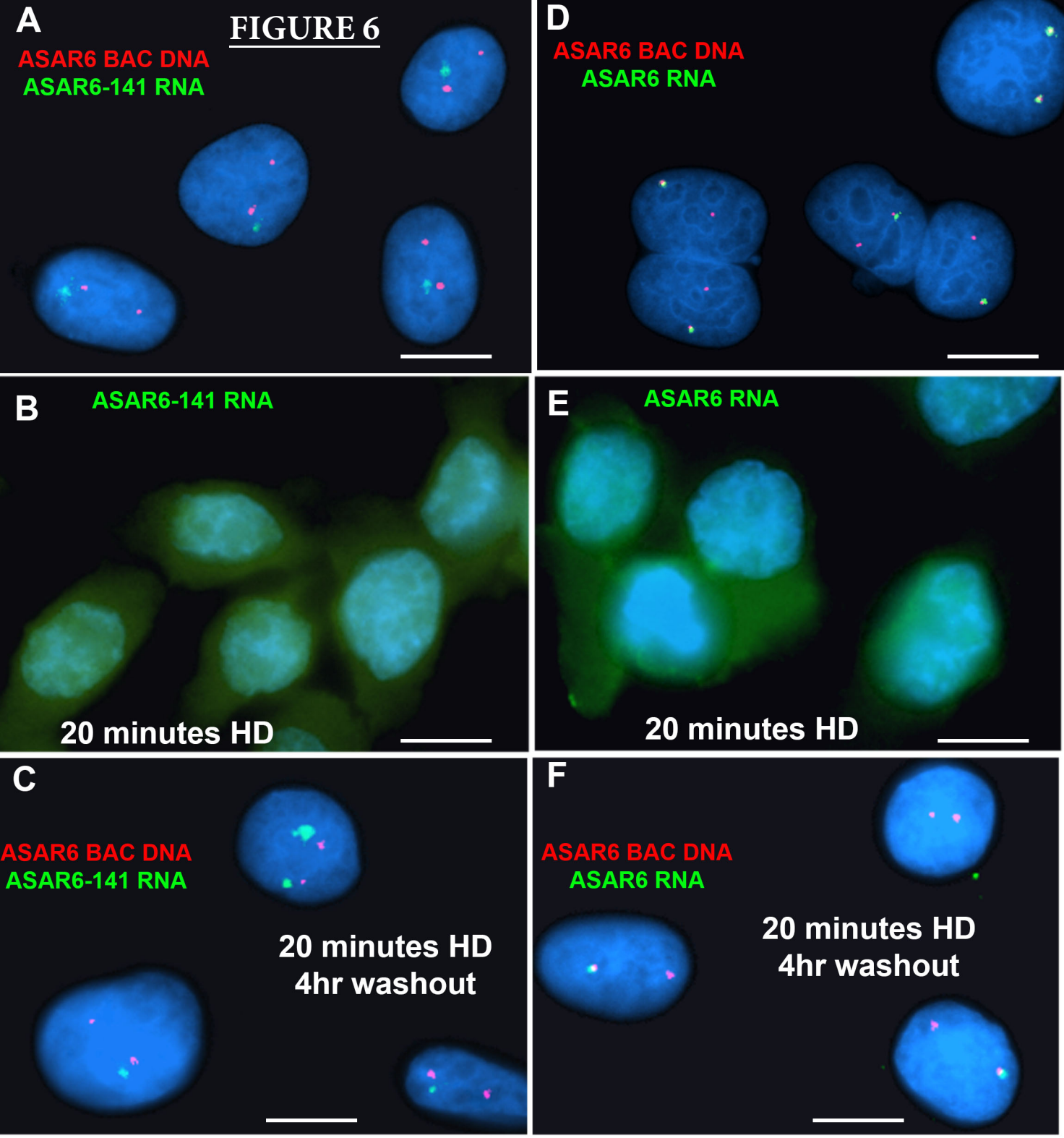
FIGURE 6
A
ASAR6 BAC DNA
ASAR6-141 RNA
D
ASAR6 BAC DNA
ASAR6 RNA
B
ASAR6-141 RNA
20 minutes HD
E
ASAR6 RNA
20 minutes HD
C
ASAR6 BAC DNA
ASAR6-141 RNA
20 minutes HD
4hr washout
F
ASAR6 BAC DNA
ASAR6 RNA
20 minutes HD
4hr washout

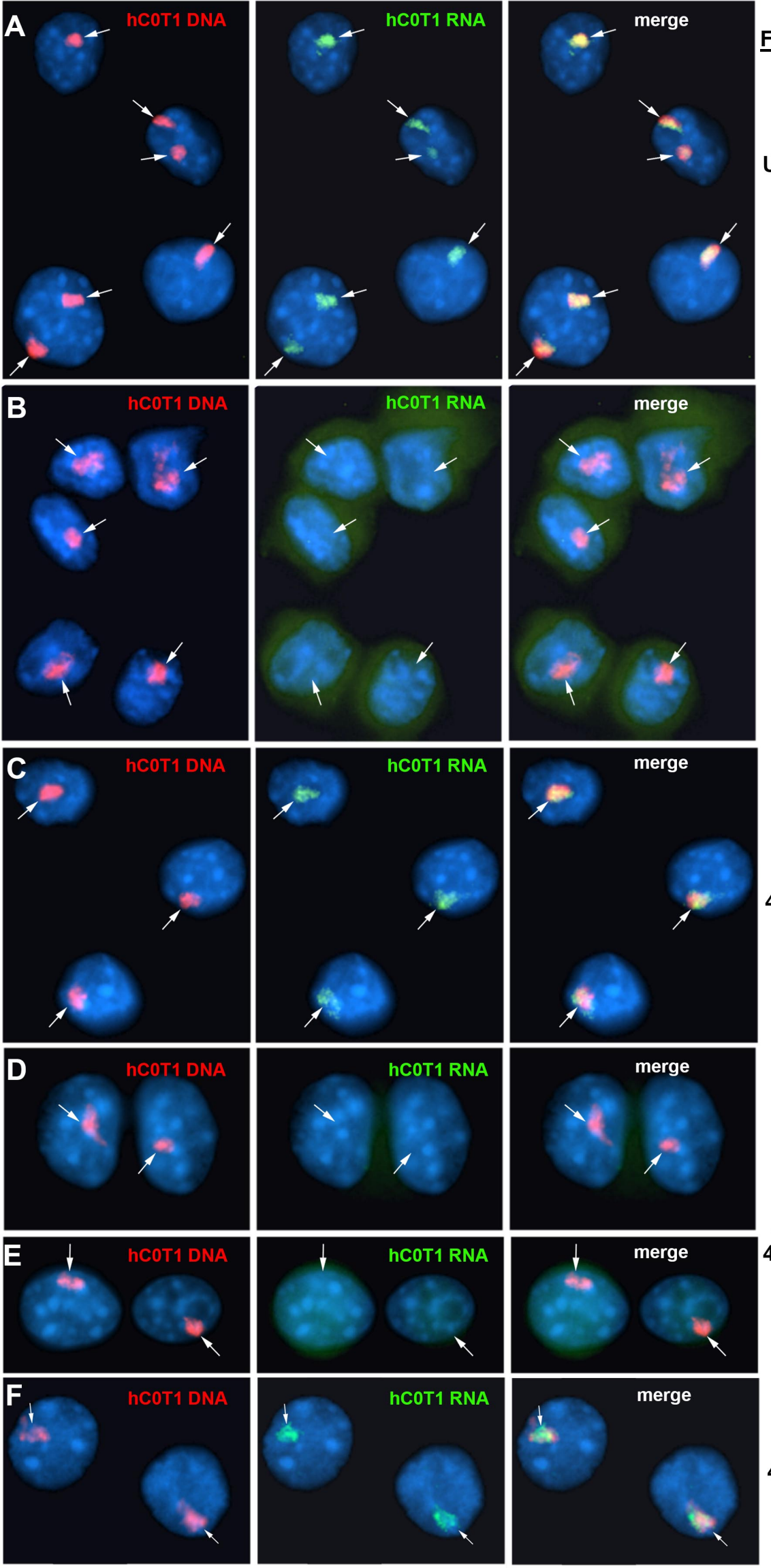
FIGURE 7
A
hC0T1 DNA
hC0T1 RNA
merge
Untreated
B
hC0T1 DNA
hC0T1 RNA
merge
20 min
4% HD
C
hC0T1 DNA
hC0T1 RNA
merge
20 min
4% HD/
4hr wash
D
hC0T1 DNA
hC0T1 RNA
merge
20 min
4% HD/
4hr wash
+ActD
E
hC0T1 DNA
hC0T1 RNA
merge
F
hC0T1 DNA
hC0T1 RNA
merge
4hr ActD

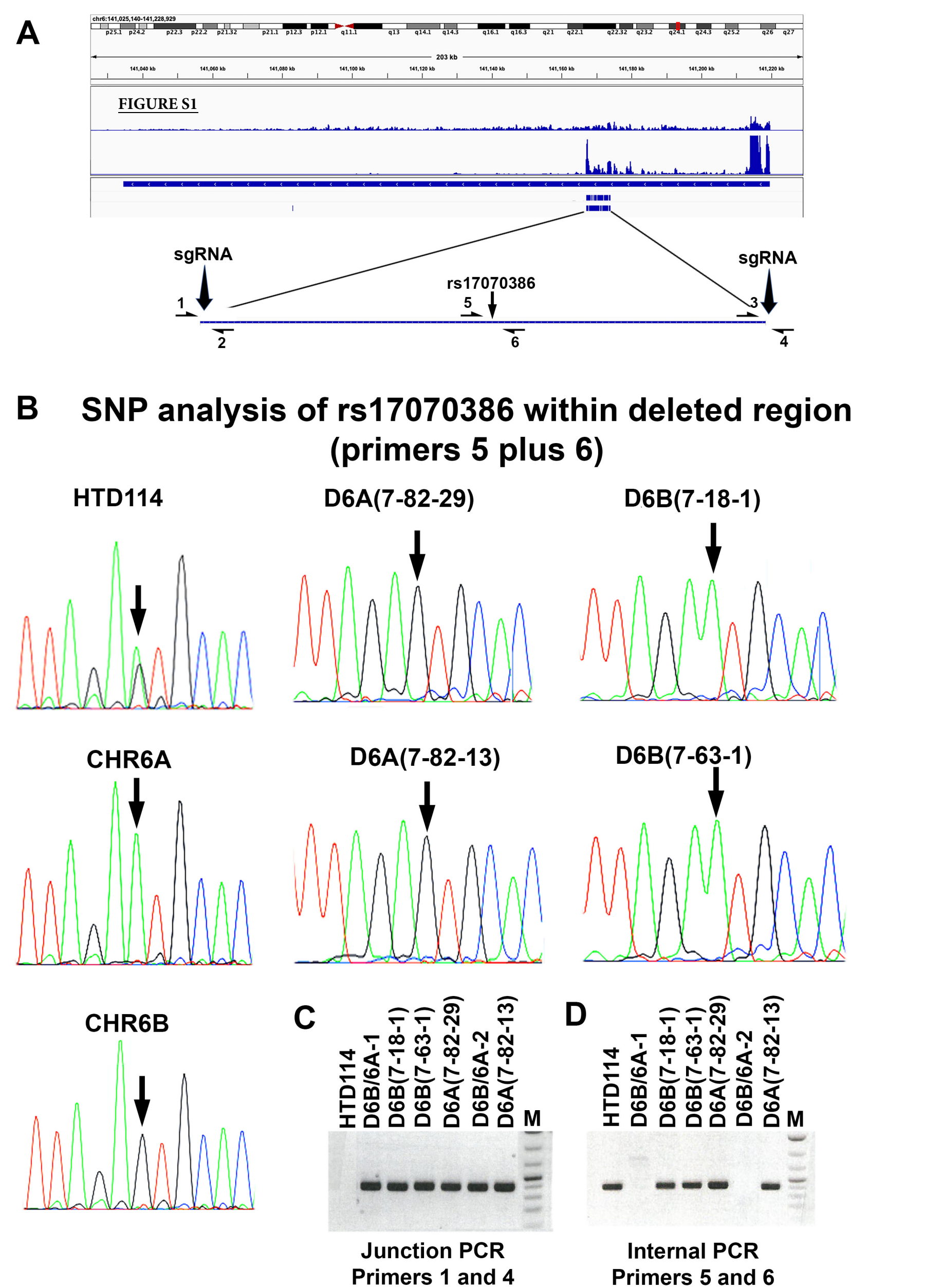
A
chr6:141,025,140-141,228,929
203 kb
FIGURE S1
sgRNA
sgRNA
rs17070386
1
2
3
4
5
6
B
SNP analysis of rs17070386 within deleted region
(primers 5 plus 6)
HTD114
D6A(7-82-29)
D6B(7-18-1)
CHR6A
D6A(7-82-13)
D6B(7-63-1)
CHR6B
C
HTD114
D6B/6A-1
D6B(7-18-1)
D6B(7-63-1)
D6A(7-82-29)
D6B/6A-2
D6A(7-82-13)
M
Junction PCR
Primers 1 and 4
D
HTD114
D6B/6A-1
D6B(7-18-1)
D6B(7-63-1)
D6A(7-82-29)
D6B/6A-2
D6A(7-82-13)
M
Internal PCR
Primers 5 and 6

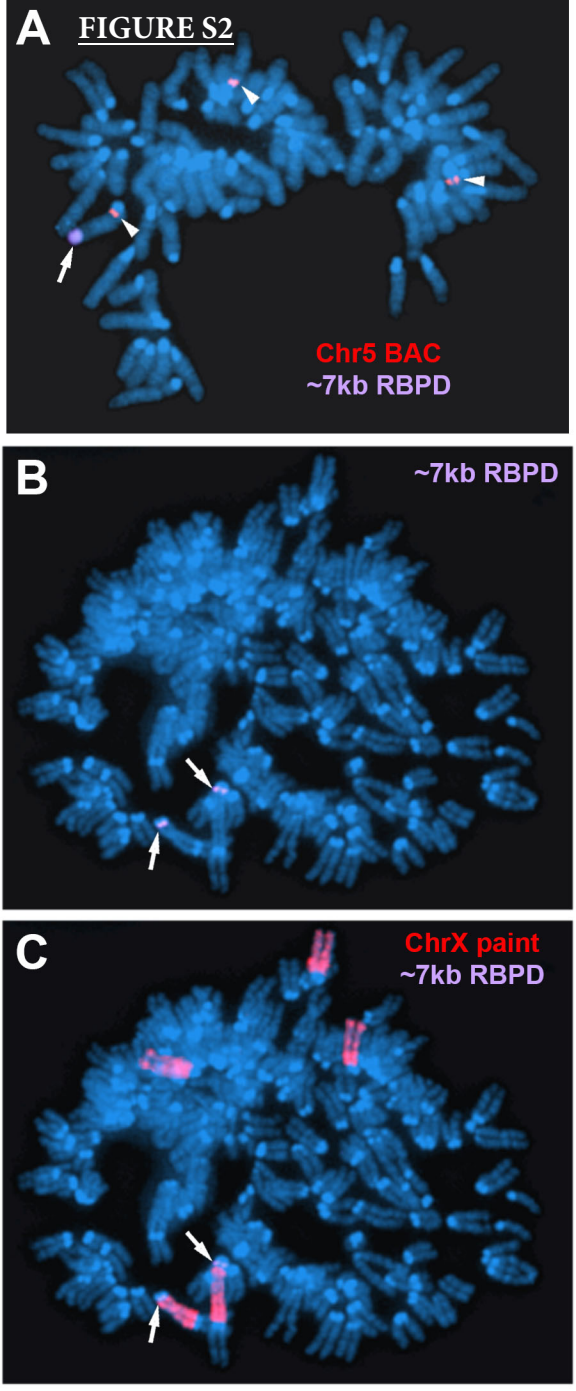
A
FIGURE S2
Chr5 BAC
~7kb RBPD
B
~7kb RBPD
C
ChrX paint
~7kb RBPD

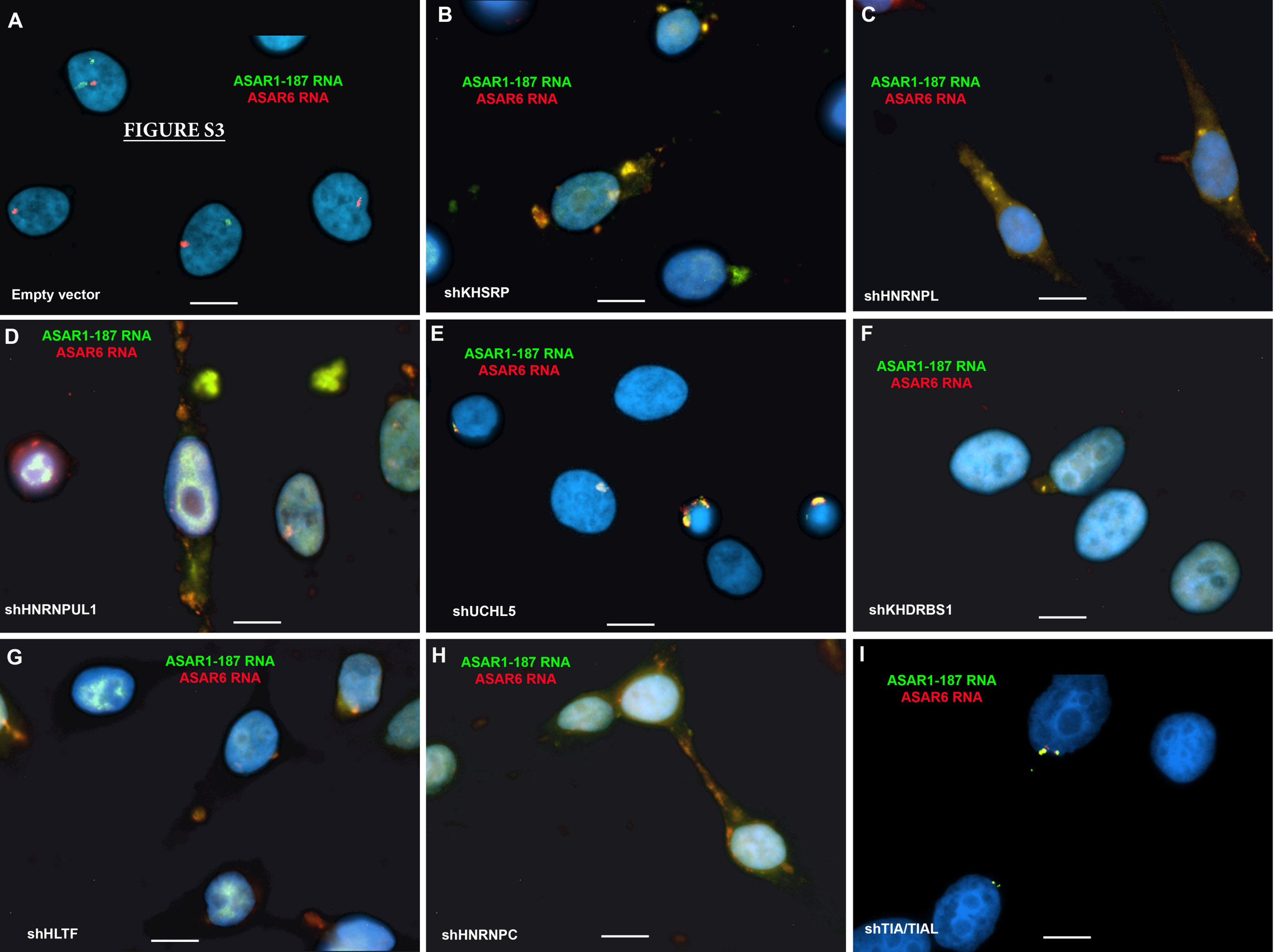
A
ASAR1-187 RNA
ASAR6 RNA
FIGURE S3
Empty vector
B
ASAR1-187 RNA
ASAR6 RNA
shKHSRP
C
ASAR1-187 RNA
ASAR6 RNA
shHNRNPL
D
ASAR1-187 RNA
ASAR6 RNA
shHNRNPUL1
E
ASAR1-187 RNA
ASAR6 RNA
shUCHL5
F
ASAR1-187 RNA
ASAR6 RNA
shKHDRBS1
G
ASAR1-187 RNA
ASAR6 RNA
shHLTF
H
ASAR1-187 RNA
ASAR6 RNA
shHNRNPC
I
ASAR1-187 RNA
ASAR6 RNA
shTIA/TIAL

FIGURE S4

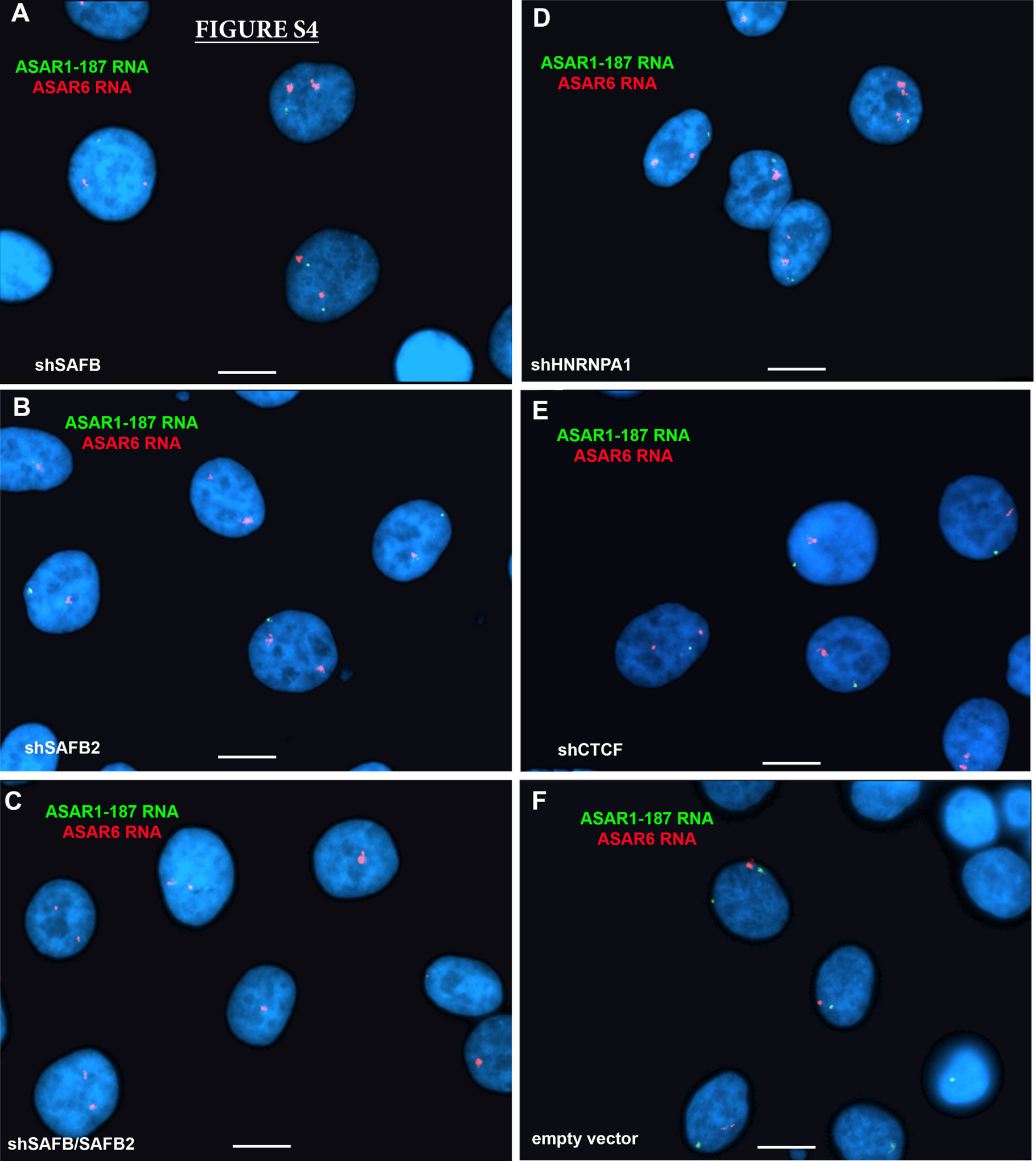
A
ASAR1-187 RNA
ASAR6 RNA
shSAFB
B
ASAR1-187 RNA
ASAR6 RNA
shSAFB2
C
ASAR1-187 RNA
ASAR6 RNA
shSAFB/SAFB2
D
ASAR1-187 RNA
ASAR6 RNA
shHNRNPA1
E
ASAR1-187 RNA
ASAR6 RNA
shCTCF
F
ASAR1-187 RNA
ASAR6 RNA
empty vector

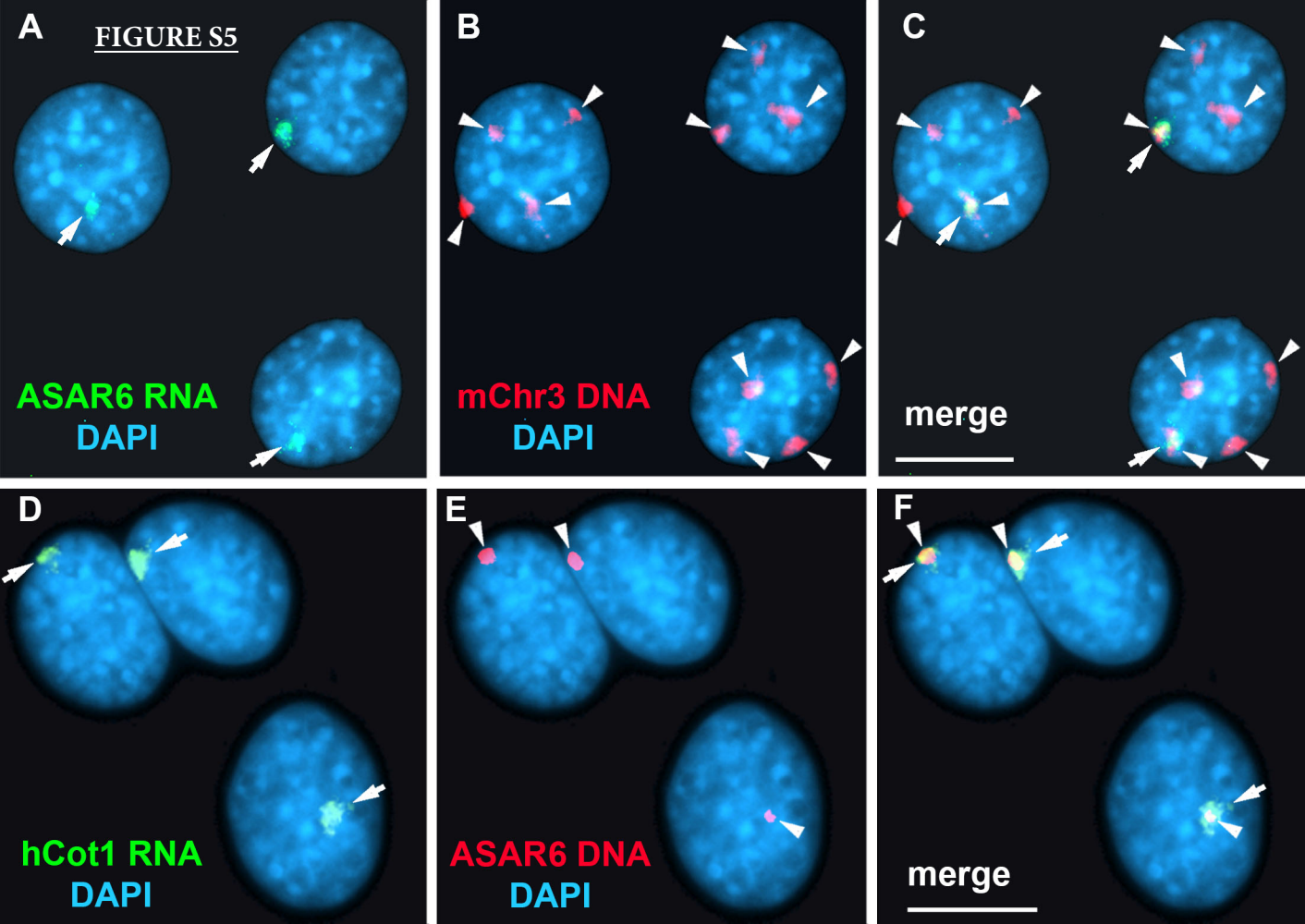
A
FIGURE S5
ASAR6 RNA
DAPI
B
mChr3 DNA
DAPI
C
merge
D
hCot1 RNA
DAPI
E
ASAR6 DNA
DAPI
F
merge